İZMİR KÂTİP ÇELEBİ ÜNİVERSİTESİ
2010
GRADUATE SCHOOL OF NATURAL AND APPLIED SCIENCES

Dynamics of Axisymmetric Drops Impacting onto Heterogeneous Surfaces

Submitted to the Graduate School of Natural and Applied Sciences in partial fulfillment of the requirements for the degree of

Master of Science

in Mechanical Engineering

by

Atalay SEÇER

ORCID 0000-0001-9944-3706

February, 2023

This is to certify that we have read the thesis **Dynamics of Axisymmetric Drops Impacting onto Heterogeneous Surfaces** submitted by **Atalay Seçer**, and it has been judged to be successful, in scope and in quality, at the defense exam and accepted by our jury as a MASTER'S THESIS.

APPROVED BY:

Advisor: **Asst. Prof. Dr. Umut Ceyhan** ……..
İzmir Kâtip Çelebi University

Committee Members:

Assoc. Prof. Dr. Utku Şentürk ……..
Ege University

Assoc. Prof. Dr. Mehmet Akif Ezan ……..
Dokuz Eylül University

Date of Defense: February 2, 2023

Declaration of Authorship

I, **Atalay Seçer**, declare that this thesis titled **Dynamics of Axisymmetric Drops Impacting onto Heterogeneous Surfaces** and the work presented in it are my own. I confirm that:

- This work was done wholly or mainly while in candidature for the Master's degree at this university.
- Where any part of this thesis has previously been submitted for a degree or any other qualification at this university or any other institution, this has been clearly stated.
- Where I have consulted the published work of others, this is always clearly attributed.
- Where I have quoted from the work of others, the source is always given. This thesis is entirely my own work, with the exception of such quotations.
- I have acknowledged all major sources of assistance.
- Where the thesis is based on work done by myself jointly with others, I have made clear exactly what was done by others and what I have contributed myself.

Signature:

_____

Date: 02.02.2023

_____

Dynamics of Axisymmetric Drops Impacting onto Heterogeneous Surfaces

Abstract

The way a droplet behaves when it lands on a surface depends on the characteristics of the surface and the flow conditions of the droplet. It can deposit, rebound, splash, etc. There is delimited research on how surface roughness and chemical composition affect the deformation of droplets upon impact, in comparison to the studies done on smooth surfaces. Our model uses two-phase flow to simulate the axisymmetric motion of droplets over surfaces with heterogeneities by combining the Navier-Stokes equations for motion with the Cahn-Hilliard equation for tracking the phase-field. We integrate the problem with a finite element solver (FEM). To accomplish this, we use piecewise linear, $P1$, triangular finite elements for the pressure components, and piecewise quadratic, $P2$, for the velocity, phase field and chemical potential, in order to integrate the governing equations. We not only discuss the interpolation types of viscosity and phase field but also suggest a new quadratic interpolant for fluids. As a starting point, we examine the effect of droplets impacting onto smooth and chemically uniform surfaces, and compare our findings with experimental results to validate our solver. We show how the maximum spreading diameter, d_{max}, after impact scales over uniform energy surfaces and compare with the literature. Dimensionless parameters Weber, Reynolds, Cahn, Capillary, Peclet numbers and density with viscosity contrasts decide the outcome on the surfaces, however, by manipulating surface energy, it is possible to control the deformation of impacting droplets, even when other parameters are held constant. We designed a wettability pattern, added roughness and observe we could change the fate of an impacting drop.

Keywords: Drop Impact, Wettability, Roughness, Finite Element Method

Heterojen Yüzeylere Çarpan Aksisimetrik Damlaların Dinamiği

Öz

Bir damlacığın yüzeye çarptığı durum, yüzeyin özellikleri ve damlacığın akış koşullarına bağlıdır. Damlacık yüzeye tutunabilir, geri tepebilir, çarparak dağılabilir vb. Pürüzsüz yüzeylerde yapılan araştırmalara kıyasla, yüzey pürüzlülüğü ve kimyasal bileşimin damlacıkların çarpışması üzerindeki etkileri hakkında sınırlı araştırma yapılmıştır. Modelimiz, hareket için Navier-Stokes denklemlerini faz alanını izlemek için Cahn-Hilliard denklemiyle birleştirerek heterojen yüzeyler üzerinde damlacıkların aksismetrik hareketini simüle etmek için iki fazlı akışı kullanır. Problemi sonlu eleman çözücüsü (FEM) ile integre ediyoruz. Bunu yapmak için, basınç bileşenleri için parçalı doğrusal, $P1$, ve hız, faz alanı ile kimyasal potansiyel için parçalı ikinci dereceden, $P2$, üçgenimsi elemanlar kullanıyoruz. Bilinen interpolasyon tiplerinin yanı sıra sıvılar için yeni bir ikinci dereceden interpolasyon öneriyoruz. Başlangıç noktası olarak, düz ve kimyasal olarak homojen yüzeylere çarpan damlacıkların etkisini inceleyerek, bulgularımızı deneysel sonuçlarla karşılaştırarak çözücümüzü doğruluyoruz. Darbe sonrası maksimum yayılma çapın d_{max} ile nasıl ölçeklendiğini ve homojen enerji yüzeyleri üzerinde nasıl değiştiğini gösteriyor ve literatürle karşılaştırıyoruz. Weber, Reynolds, Cahn, Kılcallık, Peclet sayıları ve yoğunluk ile viskozite farkları, yüzeyler üzerindeki sonucu belirler, ancak yüzey enerjisini manipüle ederek, diğer parametreler sabit tutulsa bile, çarpan damlacıkların deformasyonunu kontrol etmek mümkündür. Islanabilirlik modeli tasarladık, pürüzlülük ekledik ve çarpan bir damlanının kaderini değiştirebileceğimizi gözlemledik.

Anahtar Kelimeler: Damla Çarpması, Islanabilirlik, Pürüzlülük, Sonlu Elemanlar Metodu

Raison d'être, thou and thy warm.

Acknowledgment

So much happened in these extensive and engaging research period. But in all of this hard times my advisor, Dr. Umut Ceyhan’s warm heart has made everything easier. In our nearly 6 years of life, there has never been a day that I did not feel grateful to him. I wish we continue to keep in touch until the end of times.

I would also like to thank my family and friends for their unwavering support through all my felt like inadequate and paltry moments and for being a thin, kind shield against any social pressure mainly formed as a wrong-born moral responsibility which I think we all faced and will continue to face on this life path.

Finally, I would like to thank the family of 115 Karma for being the hand that draws me from my monotony life and my thesis. On numerous day, I was with their sincere touch and smile.

Thank you all from my heart.

Table of Contents

List of Figures

List of Tables

List of Symbols

Cn	Cahn number (ϵ/D)
Ca	Capillary number ($\mu_d U/\sigma = We/Re$)
Δ	Difference
D	Diameter, the scaling
d	Diameter
d_{max}	Maximum spreading
c	Different representation of phase-field
r	Direction on r - axes
z	Direction on z - axes
μ	Dynamic viscosity ($\mu_d \lambda_2$)
η	Chemical potential
θ_e	Equilibrium angle
γ	Surface energy density
$\boldsymbol{f}$	Body force
n	Gauss point number
∇	Gradient operator
h	Height
Ψ	Helmholtz free energy
$\mathbf{I}$	Identity tensor
P	Impact number
u_i^*	Imposed constraint at node i

J	Jacobian
E_U	Kinetic energy
$P1$	Linear space
m	Mass
m	Mesh
M	Mobility
E_η	New energy for measuring
Ω	Domain
Pe	Peclet number ($U\epsilon D/M\sigma$)
ϕ	Phase-field
ϵ	Phase change distance
p	Pressure
$P2$	Quadratic space
Re	Reynolds number ($\rho_d UD/\mu_d$)
$\boldsymbol{R}$	Right-hand side vector (knowns)
ρ	Density ($\rho_d \lambda_1$)
β	Scaling dependent on ϵ
α	Scaling dependent on ϵ
λ	Second viscosity
$\boldsymbol{s}$	The Solution to be solved (unknowns)
$\boldsymbol{K}$	Stiffness matrix
σ_{LV}	Liquid-vapor surface tension
σ_{SL}	Solid-liquid surface tension
σ_{SV}	Solid-vapor surface tension
σ	Surface tension
E_γ	Surface energy
$\boldsymbol{\tau}$	Sum of a viscosity term (deviatoric stress)

$\mathbf{T}$	Cauchy stress tensor
$\boldsymbol{T}$	Tangent stiffness matrix
t	Time
θ	Contact angle
T_h	Triangles' average edge length
λ_2	Viscosity, the value
$\boldsymbol{B}$	Vector for an need of Lagrange multiplier
$\mathbf{u}$	Velocity
U	Velocity, the scaling
u	Velocity on r - axes
w	Velocity on z - axes
ϑ_d	Volume of the droplet
We	Weber number ($\rho_d U^2 D/\sigma$)

Subscripts

a	Ambient fluid
x	Direction along x - axis
y	Direction along y - axis
z	Direction along z - axis
b	Bottom of the domain
d	Droplet
l	Linear
q	Quadratic
R	Receding
r	Residual
s	Scale

$\boldsymbol{\sigma}$	Surface tension forces
t	Trapped

Superscripts

$'$	Belongs to the mapping domain
n	Initial time step
$n+1$	Next time step
m	Initial iteration step
$m+1$	Next iteration step
$\bar{}$	Test function
T	Transpose

Chapter 1

Introduction

The impact of drops has been a prominent part of our daily lives, often manifesting through various phenomena that arise from their inherent nature which may go unnoticed. The behavior after impact can be categorized into several regimes such as deposition, prompt splash, corona splash, break-up, partial rebound and complete rebound. One of the earliest studies dates back to the late 19th century by Worthington [1, 2] about drops of liquid splashing and early 20th century by G.I. Taylor built upon Einstein's research on the flow properties of liquids containing suspended solid particles, by substituting fluid droplets for the solid particles [3], these studies have attracted a lot of attention from scholars and led to the reporting of numerous studies utilizing theoretical, experimental, and numerical techniques over the years. Examples from industry can be given as, spray cooling of surfaces to achieve efficient heat transfer [4, 5], ink-jet printing for generating droplets on demand [6], spray coating with fluid atomization which involves breaking up the coating material into small droplets [7], solder-jet technology for aircraft [8] and DNA microarrays and synthesis [9] and etc., for existing and emerging technologies. There has been an urge to control such physics and such a vast array of applications, this implies that the physical and operational parameters encompass a wide spectrum and can encompass the concept of wetting, impact dynamics, and multiphase flows: phase dynamics.

1.1 Wetting

Wetting is the ability of a liquid to adhere to a solid surface, which is determined by the interaction between the liquid and the solid at their interface and affected with surface tension. This tension force causes droplets to take on a spherical shape with no

influence by external forces [10]. The study of this phenomenon, including the attractive and repulsive forces at play, has a long history dating back to 1805 [11]. It was discovered by Poisson [12] that a continuous transition of density, rather than a sharp boundary, must be taken into account to fully understand surface tension.

Surface tension can be explained by the interaction of fluid particles with their surroundings. These interactions involve both attractive and repulsive forces. The repulsive forces can be thought of as contact forces and are relatively short-ranged, solely sensitive to the density of particles in the close vicinity. As a result, they are isotropic, meaning they act equally in all directions. On the other hand, the attractive forces are long-ranged and depend on the gradual change of particle density [13, 14].

The surface tension of a liquid - vapor interface can be comprehended by considering the balance of forces acting on the interface. When an imaginary plane is cut through the interface, perpendicular to its surface, the pressure in this direction (normal to the interface) is found to be constant. This is because the densities of both the liquid and vapor phases decrease towards the interface, causing the repulsive forces between particles to decrease. At the same time, the attractive forces between particles also decrease due to the decrease in the number of interaction partners. The result is a balance between the decreasing repulsive and attractive forces, leading to a constant pressure in the normal direction.

On the other hand, when the imaginary plane is cut through the interface tangentially to its surface, the pressure in this direction is found to decrease. This is because the repulsive forces between particles also decrease in this direction, but the attractive forces between particles decrease at a slower rate due to the greater number of interaction partners in this direction. The result is a net decrease in the pressure tangential to the interface. The integral of this pressure drop in the normal direction is called the surface tension, which is a force per unit length [15, 16].

There are several different types of wetting, including complete wetting, partial wetting, and non-wetting. Complete wetting occurs when the liquid completely covers the surface and forms a thin film on it. Partial wetting occurs when the liquid covers only part of the surface, and non-wetting occurs when the liquid does not wet the surface at all and forms beads or drops on it as shown in Figure 1.1.

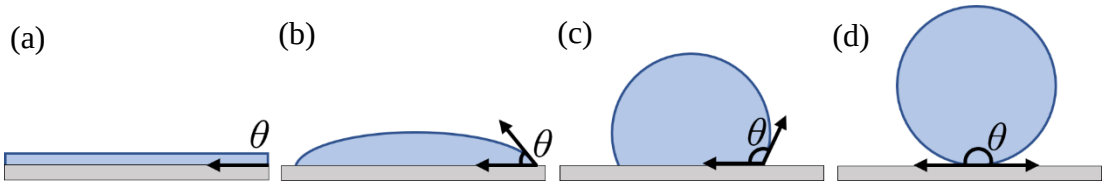

Figure 1.1: (a) perfect wetting, θ = 0, (b) partial wetting, $\theta < 90$, hydrophilic surface, (c) partial wetting θ > 90, hydrophobic surface, (d) non-wetting θ = 180.

In the drop scenario (b) and (c) the liquid is in contact with a solid surface surrounded with vapor and there are three interfaces that can be identified with surface tension: the liquid-vapor interface σ_{LV}, the liquid-solid interface σ_{SL}, and the solid-vapor interface σ_{SV}.

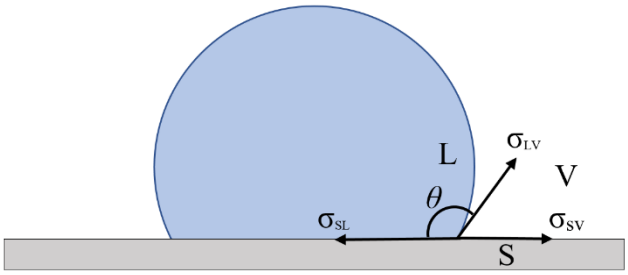

Figure 1.2: Droplet on solid surface with contact angle θ.

The relationship between surface tensions and the contact angle can be determined by analyzing Figure 1.2. The force balance in the horizontal requires

$$\sigma_{LV} \cos\theta = \sigma_{SV} - \sigma_{SL} \tag{1.1}$$

which is known as Young's condition [11] and is valid over ideal surfaces which are atomically smooth and chemically homogeneous.

Surface heterogeneity refers to the presence of different physical properties or characteristics on the surface of substrate or fluid interface. This can be caused by a variety of factors, such as variations in temperature, chemical composition, or surface roughness. Since we work on isothermal systems, last two are the scope of the thesis.

One way in which the chemical composition of a surface can affect the state of a liquid is through the forces of adhesion and cohesion through surface energy changes of the liquid-solid interface [17]. The droplet tends to have a greater attractive force and is more prone to wetting for high energy surfaces, while a surface with a chemical composition that generates a lower surface energy, the liquid has a weaker attractive force and will be less prone to wetting.

The modification can be made simply by applying a coating as presented in Figure 1.3, (a) with a red line or by a treatment to make it more hydrophobic or hydrophilic that changes its surface energy. For example, a hydrophobic coated surface make it more water-repellent, while a hydrophilic coating can be applied to make it more water-attracting [18, 19].

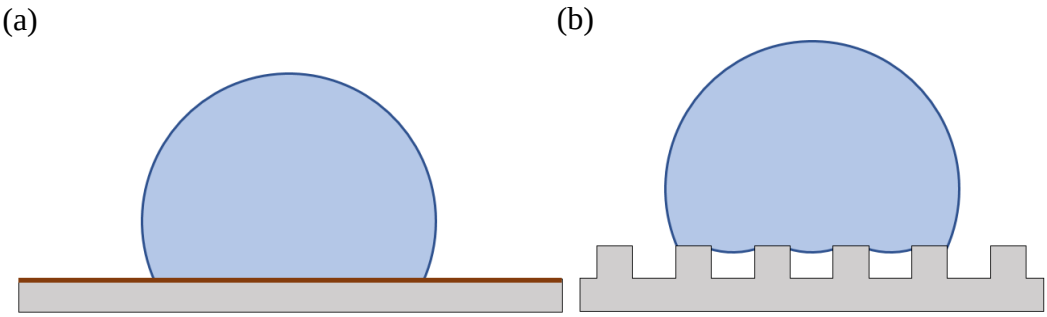

Figure 1.3: Two main wetting states with the different surface heterogeneities.

On the other hand, the presence of particles or impurities of the surface, or in by a simple roughness under the fluid can chance the behavior. The roughness on the surface may cause the liquid to begin wetting the surface before the main impact, resulting in a loss of internal energy. The increase in the contact area between the droplet and the surface leads to a less impact force while doing that can also cause the flow to become chaotic and it increases the drag forces acting on the fluid particles in the droplet, which can reduce its impact velocity before the full impact of its body [20]. In the Figure 1.3 (b), we show the influence of structures on wetting which is the well-known Cassie-Baxter state [21].

After discussing wetting, it is important to discuss impact dynamics as the rest of the thesis is about this behavior.

1.2 Drop Impact

We start this section by describing different regimes observed after impacting drops. Six distinct regimes are reported through the experimental studies as shown in Figure 1.4 and this rich physics has been explained by many researchers [22-24].

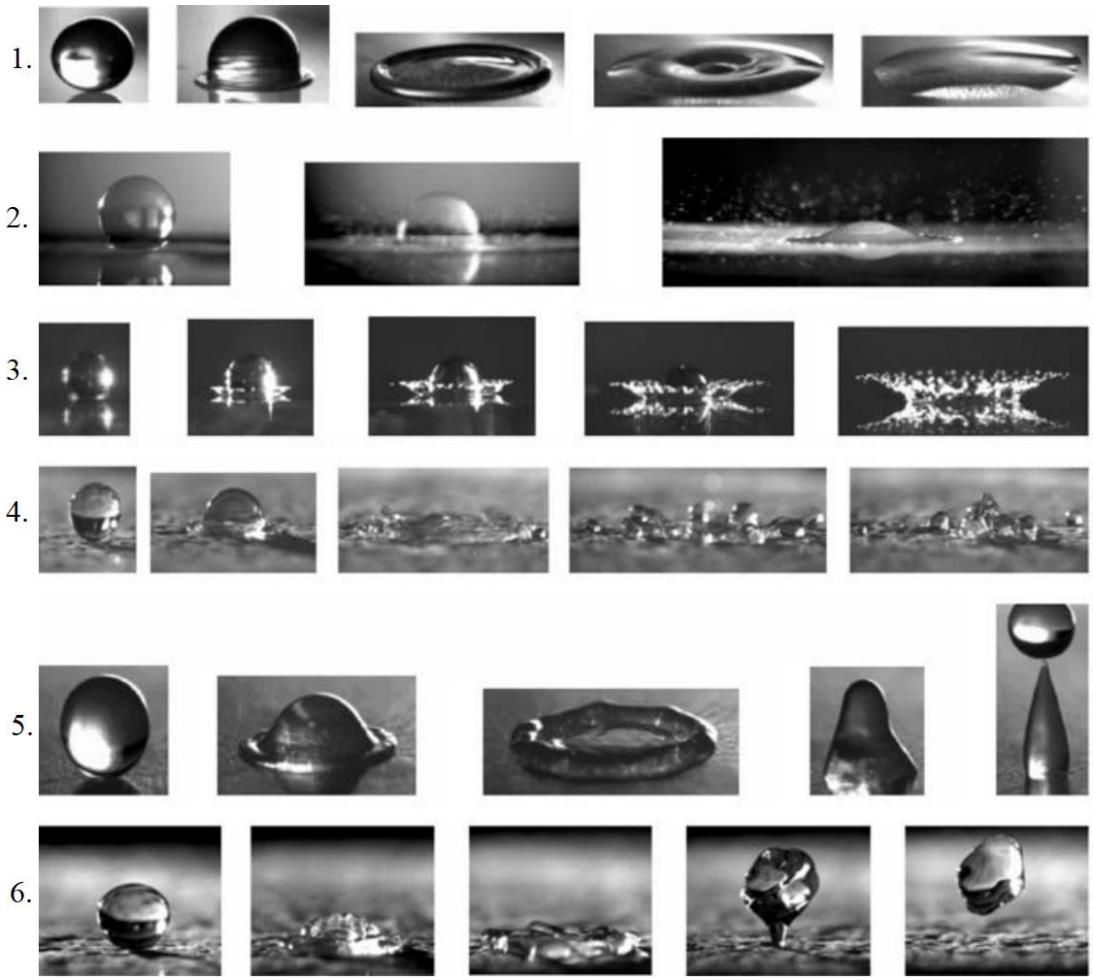

Figure 1.4: Different regimes of droplets impacting on substrate, adapted from Rioboo et al. (2001) [22].

In the order shown 1 through 6 in Figure. 1.4, we itemize all cases below.

1. Deposition is the process in which a droplet attaches to a surface upon impact, without breaking apart. This typically happens when a small droplet with low velocity hits a smooth and wet surface.

2. When a drop hits a rough surface, it may produce "prompt splash," a process in which droplets are generated at the point of contact between the solid, gas, and liquid. This phenomenon is characterized by the drop's high outward velocity at the start of spreading on the surface.

3. If the surface tension of the wall is reduced, it may cause the liquid layer to separate from the wall, resulting in a "corona splash."

4. When a liquid retracts from its maximum spread on a wetting surface, "receding breakup" can occur. The reason for this is that as the droplet retracts, the angle of contact decreases, resulting in some of the droplet remaining on the surface. On superhydrophobic surfaces, the retracting drop can break into smaller droplets called satellite droplets during both the spreading and retracting phases. This may be due to capillary instability, and these satellite droplets can also break apart.

5 - 6. A drop that recedes after impact can produce either a "partial rebound" or "complete rebound" phenomenon. During the receding process, the drop's kinetic energy causes the liquid to rise up and form a vertical column. When a droplet only releases a portion of itself from the surface while remaining attached, it is called a partial rebound. If the droplet completely detaches from the surface, it is known as a complete rebound. The type of rebound that takes place is determined by the angle of contact as the droplet recedes from the surface. A partial rebound happens when the angle is low, while a complete rebound occurs when the angle is high, provided that the drop has sufficient kinetic energy.

When all impacts are considered, for dimensional parameter groups to perform a certain phenomenon, their quantities must be in certain thresholds or pass to achieve another. This is summarized by Rioboo et al. [22] in the following table 1.1. In the order shown in the first column, $\mathbf{u}$ is the drop's impact velocity, D is the diameter of the drop, σ is the surface tension, μ is the viscosity and θ is the contact angle with the surface. The arrow directions show with the increase or decrease of the parameter, observance of the corresponding regime may be possible.

Table 1.1: Effect of parameters on impact regime.

Increase of	Deposition	Prompt splash	Corona splash	Receding breakup	Partial rebound	Complete rebound
u	↓	↑	↑	↑	↑	
D		↑				
σ		↓	↓	↑	↑	
μ	↑	↓	↓	↓		↑
θ	↓	↑		↑	↑	↑

Before getting involved with the body of thesis we need to clarify the last but the most important topic for thesis: The multiphase flow, phase dynamics. We first give fundamental definitions with the concept then there are several approaches that can be used to model droplet phenomena, these continue with the numerical and theoretical models.

1.3 Multiphase Flows: Phase Dynamics

Multiphase flow refers to the movement of materials with more than one thermodynamic phase at the same time or two different fluids at the same phase. A phase is a substance that has a distinctive chemical or physical property. The specific property used to identify the phase can vary depending on the purpose of the research. For example, in carbon chemistry, the crystal structure is used to identify the two stable phases of carbon: diamond and graphite [25]. The electrical polarization is frequently employed as a means of identifying different phases in the study of ferroelectric ceramics [26]. In the field of fluid mechanics, the proportion of various substances is often employed as a means of classifying different phases. This is because these substances possess distinct fluid characteristics, such as viscosity, thermal conductivity and capillarity. Additionally, the density of a fluid which is closely tied to its state of matter is used to differentiate between liquid and gaseous phases.

A phase transformation refers to a change in the physical or chemical properties of a substance that occurs due to a change in the environment. This can include changes in temperature, pressure, composition, or other external factors. When involving multiple substances, the behavior of the system can become more complex [27]. Equilibrium

thermodynamics is an important tool for understanding the equilibrium state of immiscible fluids separated by a thin region, known as the interface. With the advancement of technology, several simulation models have been developed over the years to numerically solve these type of problems. These models allow us to better understand and predict the behavior of multiphase systems, and are widely used in various fields such as chemical and mechanical engineering. In the next step, we will delve deeper into the different types of models and their applications in modeling multiphase flows.

Two types of phase dynamics mentioned over the years and many techniques have been developed to model and simulate the simultaneous flow of materials with multiple phases and components. These methods can be divided into two categories: those that track the movement of the interface between phases, and those that capture the properties of the interface [28]. In the following Figure 1.5, all types of methods could be seen.

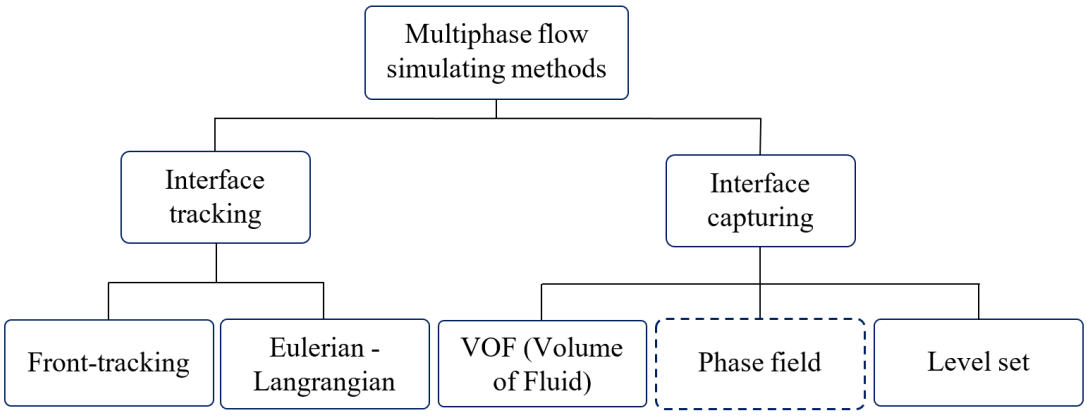

Figure 1.5: Diagram of multiphase flow methods.

The interface-tracking method tracks the interface by aligning computational nodes along the interface and moving the mesh with the fluid flow. This method provides a very accurate description of the interface because it explicitly traces the movement of the interface. However, it requires the use of sophisticated re-meshing techniques, which can be computationally expensive. Furthermore, when dealing with problems that entail major topological changes, such as interface pinch-off and connection, additional controls may be required to update the mesh. Currently, solving three-

dimensional issues with topological transitions remains challenging when using interface-tracking methods.

Interface-capturing methods involve the identification of different phases by introducing extra variables, while the entire fluid domain is included within the computation grid. These methods tend to produce less precise interface representations compared to interface-tracking methods, even when using similar spatial mesh sizes. However, they are relatively easy to implement and computationally efficient since there is no need to frequently update the mesh. Additionally, they can handle topological transitions without the need for special procedures.

Front-tracking is a particle-based method, meaning that it represents the interface as a set of discrete particles that move with the fluid flow. These particles are connected by springs to form a mesh, which is used to interpolate the properties of the interface such as surface tension and surface velocity.

The volume-of-fluid (VOF) method [29] is among the early versions of the interface-capturing methods. It employs the proportion of one fluid component in each cell for identifying different phases and does not track the movement of the interface directly, but instead estimates the location of the interface based on the properties of the fluids on either side of it but fails to capture some of the physics.

Phase field methods capture the boundary between two immiscible fluids [30]. These methods can compute topological changes in the interface, such as the formation and breakup of drops, more naturally, and thus have been successfully applied to multi-component fluid flows involving large interface deformations. They are based on partial differential equations describing the phase field's evolution over time and are a continuous function, rather than a discrete set of points or lines so that they can capture the small-scale features of the interface more accurately. They do not require ad hoc rules or sophisticated re-meshing techniques to update the mesh when the topology of the interface changes. However, they can be more computationally expensive to implement than other methods. It is the model that we use in this study.

In the level-set methods, the basic idea is to represent the interface as a scalar function, called the level-set function, which is defined on the entire computational domain. The

level-set function is chosen such that its zero contour represents the interface of interest and it changes with the flow of the velocity field, which is controlled by equations of the Hamilton-Jacobi type [31].

It's important to note that, depending on the context and the specific application of the method, the distinction between capturing and tracking may not be clear-cut, and some methods may be considered to be doing both capturing and tracking and depending on the specific application, some methods may also be more appropriate than others, and that the specific method chosen depends on the details of the problem being studied, such as the nature of the fluids, the complexity of the geometries, the ratio of densities and viscosities, among other factors.

Phase-field models can be represented by a scalar field, which is a function that maps a point in space to a scalar value. The evolution of the concentration field is described by the Korteweg, Allen-Cahn or Cahn-Hilliard or with some Spectral Methodized equations, while the motion of the fluids is described by the Navier-Stokes equations of motion. A diagram for governing equations for phase-field methods is shown in Figure 1.6.

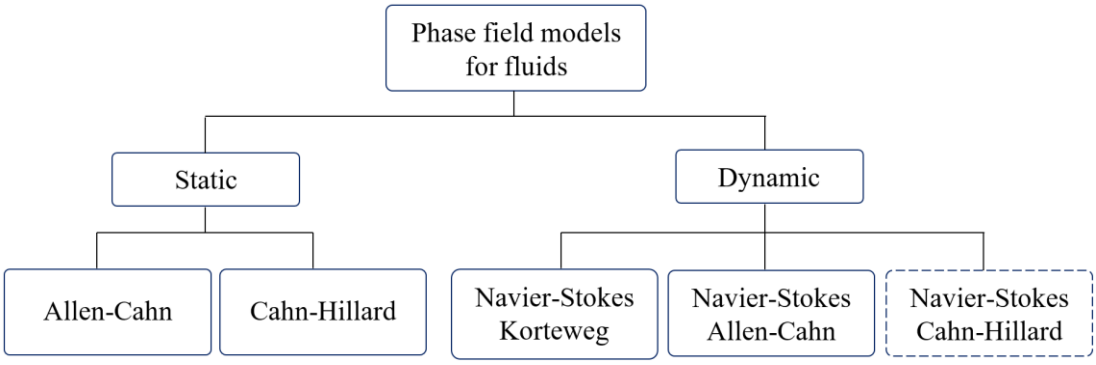

Figure 1.6: Diagram of model equations in phase-field.

Briefly, Korteweg method is based on the Korteweg stress tensor, which is a generalization of the viscous stress tensor used in the Navier-Stokes equations [32]. Cahn-Hilliard, which keeps track of a scalar field called the phase field varies smoothly across the interface between different phases [33]. In Allen-Cahn model is then derived

by a simplification from the Cahn-Hilliard with conserved order parameters [34]. We can either solve them in the steady field means statically or unsteady field dynamically.

1.4 Motivation

In recent years, there has been a growing interest in understanding the behaviour of droplets and flows in particular, as they are prevalent in many technological applications. However, the research on the effects of surface roughness and chemically heterogeneous surface on droplets impacting the surface is limited compared to studies on smooth surfaces. This thesis aims to study the behaviour of droplets impacting surfaces with heterogeneities, specifically chemically heterogeneous surface and added surface roughness. By understanding the physics behind droplet-surface interactions, we can gain insight into how to design and control these interactions for various technological applications. Furthermore, developing a multiphase flow model that can accurately predict the behaviour of droplets and droplet-surface interactions, have the potential to lead to the design and can pave the way for more efficient and effective industrial processes.

The organization of the thesis is as follows. In Chapter 2, we state our problem, introduce all the constitutive models and the derivation of coupled Navier-Stokes and Cahn-Hilliard equations and finalize the governing equations. In the following Chapter 3, the numerical technique we use to reduce to their weak forms with finite element method procedure is given. In Chapter 4, we show our solver’s validation results for both water and ethanol droplets, various regimes and we give the scaling law for all our computed data of drops' maximum spreading and compare with the literature. Then, our way to control the deformation by either with a heterogeneous wettability pattern or the presence of the surface roughness is given in Chapter 5. In the final Chapter 6, we conclude the study with our summation of findings.

Chapter 2

Model Problem

Initially, we have a spherical droplet surrounded with an ambient fluid over an isothermal solid substrate in an axisymmetric system seen in Figure 2.1. Both of the fluids have their unique density and viscosity values. The phase represented from +1 to -1 means a transition from drop to ambient fluid and on the surface of the drop there happens a sharp transition to this phase change. Since we only deal with the impact its velocity is given as it is ready to impact. During that surface tension and wettability plays an important role in deciding which phenomenon occurs.

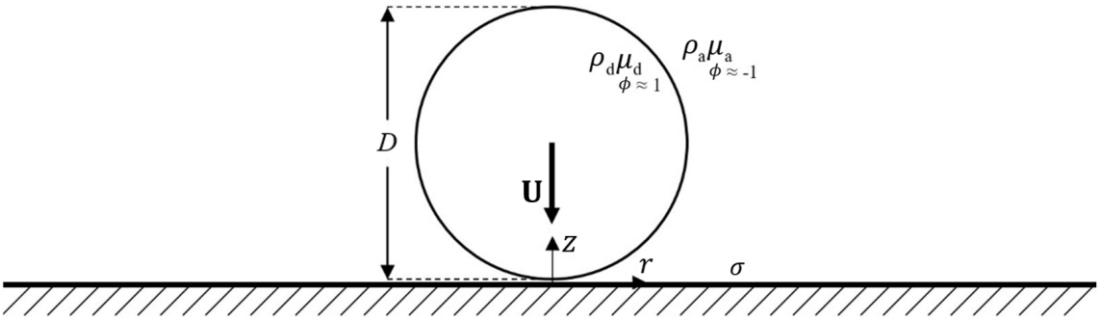

Figure 2.1: Problem domain.

The motion of fluid particles are governed the continuity equation and linear momentum balance. We first define the continuity in the form as

$$\frac{\partial \rho}{\partial t} + \nabla \cdot (\rho \mathbf{U}) = 0. \tag{2.1}$$

For an incompressible flow, density is constant does not change with time even though it varies from one phase to another, (2.1) can be reduced to

$$\nabla \cdot \mathbf{U} = 0. \tag{2.2}$$

The linear momentum balance requires

$$\rho \frac{\mathrm{D}\mathbf{U}}{\mathrm{D}t} = \nabla \cdot \mathbf{T} + \boldsymbol{f} \tag{2.3}$$

where

$$\mathbf{T} = -\nabla p + \nabla \cdot \boldsymbol{\tau} \tag{2.4}$$

is the Cauchy stress tensor with following constitutive law (pressure term is excluded) and is given by

$$\boldsymbol{\tau} = \left(\lambda + \frac{2}{3}\mu\right)(\nabla \cdot \mathbf{U})\mathbf{I} + \mu\left(\nabla\mathbf{U} + (\nabla\mathbf{U})^{\mathrm{T}} - \frac{2}{3}(\nabla \cdot \mathbf{U})\mathbf{I}\right). \tag{2.5}$$

The use of (2.2) reduces (2.5) to

$$\boldsymbol{\tau} = \mu(\nabla\mathbf{U} + (\nabla\mathbf{U})^{\mathrm{T}}). \tag{2.6}$$

Defining $\boldsymbol{f}$ to be the summation of surface tension forces resulting from the shape of the interface between the phases, $\boldsymbol{f}_{\sigma}$, and body forces, we only consider the $\boldsymbol{f}_{\sigma}$ as the effect of gravity is small for small scale drops. The Navier-Stokes equations of motion then can be written as

$$\rho \frac{\mathrm{D}\mathbf{U}}{\mathrm{D}t} = -\nabla p + \nabla \cdot \left(\mu(\nabla\mathbf{U} + (\nabla\mathbf{U})^{\mathrm{T}})\right) + \boldsymbol{f}_{\boldsymbol{\gamma}}. \tag{2.7}$$

There are various surface tension models for the phase-field methods,

$$\boldsymbol{f}_{\sigma_1} = \epsilon^2 \nabla \cdot (|\nabla\phi|^2\mathbf{I} - \nabla\phi \otimes \nabla\phi), \qquad \boldsymbol{f}_{\sigma_2} = \eta\nabla\phi, \tag{2.8 a, b, c, d, e}$$

$$\boldsymbol{f}_{\sigma_3} = -\phi\nabla\eta, \qquad \boldsymbol{f}_{\sigma_4} = \epsilon^2\nabla\cdot\left(\frac{\nabla\phi}{|\nabla\phi|}\right)|\nabla\phi|\nabla\phi,$$

$$\boldsymbol{f}_{\sigma_5} = \epsilon^2\nabla\cdot(\nabla\phi\otimes\nabla\phi\,).$$

We use the $\boldsymbol{f}_{\sigma_2}$ due to the computational ease. Different surface tension forces are used time to time to cover different physical aspects of the models [35].

In (2.7), ρ and μ can be defined as both function of phase field ϕ or concentration c. The reason behind this is that there are two ways to describe incompressible flow of immiscible binary fluids existence numerically. It's either difference [36] or the fraction of one of the concentrations [35],

$$\phi = \frac{m_1 - m_2}{m_1 + m_2}, \qquad c = \frac{m_2}{m_1 + m_2}. \tag{2.9 a, b}$$

Here m_1 and m_2 are the mass of the fluids. We again note that $-1 < \phi < 1 < 1$ and $0< c < 1$. The values on the left extreme denote pure droplets while the value on the right extreme denotes the ambient fluid. A representative phase-field transition from droplet to ambient is shown in Fig. 2.2.

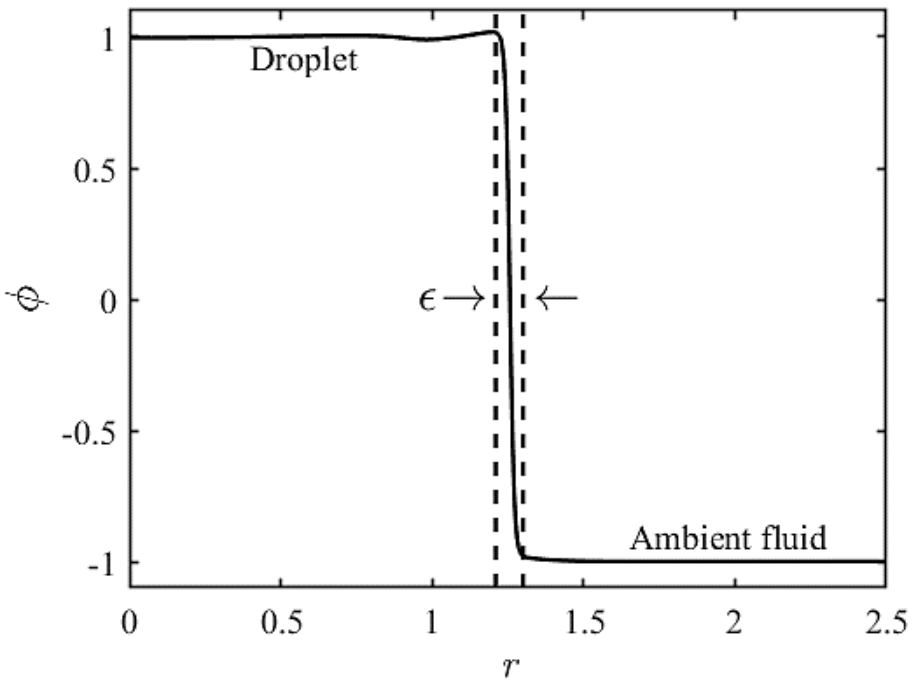

Figure 2.2: ϕ concentration field varies from -1 to 1. There happens a sharp transition to this phase change within a distance ϵ.

Depending on the approach to concentrations, equations adapt to them. Let's assume ρ_d and ρ_a are the density contrast [30, 35] defined as,

$$\rho(c) = \rho_d c + \rho_a(1-c), \qquad \rho(\phi) = \rho_d\left(\frac{1+\phi}{2}\right) + \rho_a\left(\frac{1-\phi}{2}\right). \quad \text{(2.10 a, b)}$$

Similarly μ_d and μ_a are the viscosity contrast,

$$\mu(c) = \mu_d c + \mu_a(1-c), \qquad \mu(\phi) = \mu_d\left(\frac{1+\phi}{2}\right) + \mu_a\left(\frac{1-\phi}{2}\right). \quad \text{(2.11 a, b)}$$

In this study, we use the phase-field ϕ, but we give place to both of the equations in following.

The variation of the phase-field is governed by the Cahn-Hilliard equations and given as

$$\frac{\mathrm{D}\phi}{\mathrm{D}t} = M\nabla^2\eta \qquad (2.12)$$

where η is the chemical potential defined as the variational derivative of the well-known functional of Ginzburg–Landau free energy [37]

$$f = \beta\Psi(\phi) + \frac{\alpha}{2}|\nabla\phi|^2 \qquad (2.13)$$

with respect to phase field. It is defined as

$$\eta = \beta\Psi(\phi) + \alpha\nabla^2\phi. \qquad (2.14)$$

In (2.12), M is the phase field dependent non-negative mobility and can also depend on both concentrations or phase-field as

$$M(c) = c(1-c), \qquad M(\phi) = 1-\phi^2, \qquad \mathrm{M} = 1. \qquad \text{(2.15 a, b, c)}$$

When mobility varies, the Cahn-Hilliard dynamics is influenced by diffusion at the interface and when mobility is constant, it is influenced by bulk diffusion.

Following equation is the binary fluid assumption that have a specific Helmholtz free energy (also known as double-well in the bulk potential) which is based on the work of Cahn & Hilliard [33]. It's change in the interface given in Figure 2.3.

$$\Psi(\mathrm{c}) = \frac{1}{4}c^2(1-c^2), \qquad \Psi(\phi) = \frac{1}{4}(\phi^2-1)^2. \tag{2.16 a, b}$$

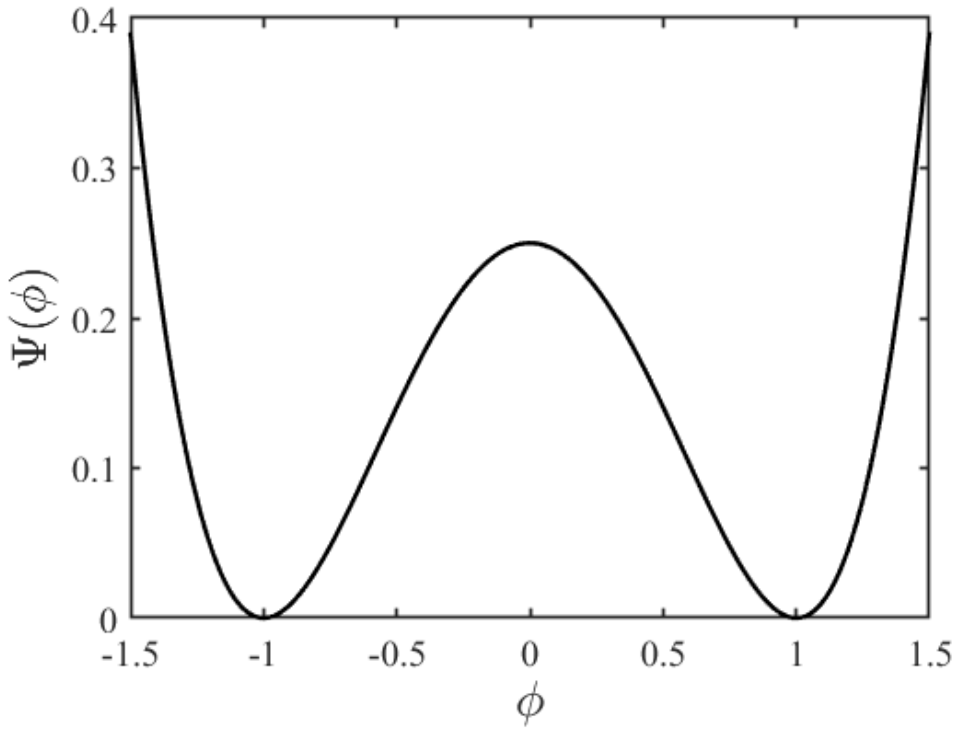

Figure 2.3: Double well potential.

2.1 Interpolation of Density and Viscosity

Equation (2.10 b) and (2.11 b) are derived from the linear interpolation across the interface, but in the harmonic interpolation the variable density and viscosity is used differently. In the harmonic equation used by Joseph & Renardy (1993) [38], the interpolation is defined as

$$\frac{1}{\rho(\phi)} = \frac{1+\phi}{2\rho_d} + \frac{1-\phi}{2\rho_a}, \tag{2.17}$$

$$\frac{1}{\mu(\phi)} = \frac{1+\phi}{2\mu_d} + \frac{1-\phi}{2\mu_a}. \tag{2.18}$$

The harmonic interpolation is preferred because the solution of the Cahn-Hilliard equation does not abide by the maximal principle [35]. Linear interpolation may not prevent the solution from approaching zero. However, the harmonic interpolation guarantees that the solution remains bounded away from zero due to its L^{∞} -bound property [39].

The phase field transition from droplet to outside fluid is from 1 to -1 and the transition during the numerical integration does not guarantee that ϕ remains always above -1. In this case, the linear interpolation of density results with negative values which is not physical; this may end up with diverging solutions. One of the interpolation techniques to alter this problem is the use of harmonic interpolation as shown in Figure 2.2. The implementation of this interpolation is difficult though in the finite element method. To ease the implementation as well as providing positivity preserving scheme, we propose a new interpolation for both density and viscosity. We call it quadratic interpolation and define as

$$\rho(\phi) = \frac{\phi^2(\rho_d + \rho_a)}{4} + \frac{\phi(\rho_d - \rho_a)}{2} + \frac{(\rho_d + \rho_a)}{4}, \tag{2.19}$$

$$\mu(\phi) = \frac{\phi^2(\mu_d + \mu_a)}{4} + \frac{\phi(\mu_d + \mu_a)}{2} + \frac{(\mu_d + \mu_a)}{4}. \tag{2.20}$$

We show this interpolation in Figure 2.4 with solid line. Our proposal is between linear and harmonic represented as linear line, it is also positive at all times. Dashed and dot-dash lines represent linear and harmonic interpolations of density, respectively.

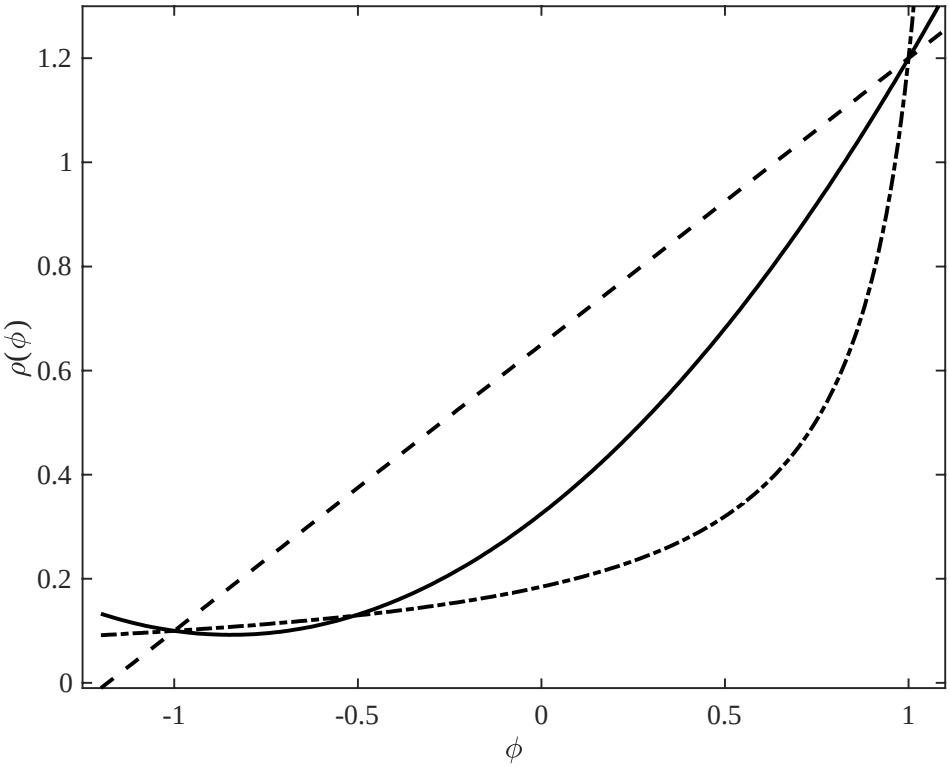

Figure 2.4 A representative density variation with different density interpolations for ρ_d = 1.2, ρ_a= 0.1, --: linear, -.-: harmonic, -: quadratic interpolations.

Equations (2.19) and (2.20) also provide us with the use of lower density contrast which is not computationally simple to achieve with linear interpolation.

Another approach is the use of Boussinesq approximation [40], which only considers the effect of the density difference between the liquid and gas phases on the body force term of the Navier-Stokes equations and ignores it in the inertia term. The linear momentum balance can then be written as

$$\rho_o \frac{\mathrm{D}\mathbf{U}}{\mathrm{D}t} = -\nabla p + \nabla \cdot \left(\mu(\nabla \mathbf{U} + (\nabla \mathbf{U})^{\mathrm{T}})\right) + \eta \nabla \phi + \frac{1+\phi}{2}\Delta\rho \mathbf{g}. \qquad (2.21)$$

The term $\rho_o = (\rho_d + \rho_a)/2$ represents the average density and if this term is modified by including the density difference as an additional body force term, it will account for the equivalent gravitational effect caused by the density difference. This technique is simple to implement as it does not add extra non-linearity to the inertial terms.

2.2 Finalized System of Equations

We, now, write the governing equations in component and open form, but in axisymmetric system. The r and z momentum after the use of continuity equation turn in to a form less known in the literature as

$$\rho^*\left(\frac{\partial u^*}{\partial t^*}+u^*\frac{\partial u^*}{\partial r^*}+w^*\frac{\partial u^*}{\partial z^*}\right)=-\frac{\partial p^*}{\partial r^*}+\frac{1}{r^*}\frac{\partial}{\partial r^*}\left(r^*2\mu^*\frac{\partial u^*}{\partial r^*}\right)+\frac{\partial}{\partial z^*}\left(\mu^*\left(\frac{\partial u^*}{\partial z^*}+\frac{\partial w^*}{\partial r^*}\right)\right)-2\frac{\mu^*u^*}{r^{*2}}+\eta^*\frac{\partial\phi}{\partial r^*}, \tag{2.22}$$

$$\rho^*\left(\frac{\partial w^*}{\partial t^*}+u^*\frac{\partial w^*}{\partial r^*}+w^*\frac{\partial w^*}{\partial z^*}\right)=-\frac{\partial p^*}{\partial z^*}+\frac{1}{r^*}\frac{\partial}{\partial r^*}\left(r^*\mu^*\left(\frac{\partial u^*}{\partial z^*}+\frac{\partial w^*}{\partial r^*}\right)\right)+\frac{\partial}{\partial z^*}\left(2\mu^*\frac{\partial w^*}{\partial z^*}\right)+\eta^*\frac{\partial\phi}{\partial z^*}. \tag{2.23}$$

The continuity is defined by

$$\frac{\partial(r^*u)}{\partial r^*}+\frac{\partial w^*}{\partial z^*}=0, \tag{2.24}$$

and the Cahn-Hillard and chemical potential equations are

$$\frac{\partial\phi}{\partial t^*}+u^*\frac{\partial\phi}{\partial r^*}+w^*\frac{\partial\phi}{\partial z^*}=M\left(\frac{1}{r^*}\frac{\partial}{\partial r^*}\left(r^*\frac{\partial\eta^*}{\partial z^*}\right)+\frac{\partial^2\eta^*}{\partial z^{*2}}\right), \tag{2.25}$$

$$\eta^*=\beta(-\phi+\phi^3)-\alpha\left(\frac{1}{r^*}\frac{\partial}{\partial r^*}\left(r^*\frac{\partial\phi}{\partial z^*}\right)+\frac{\partial^2\phi}{\partial z^{*2}}\right). \tag{2.26}$$

To non-dimensionalize our model problem, we use the following scales:

$$r^* = Dr, \qquad z^* = Dz, \qquad u^* = Uu, \qquad w^* = Uw, \qquad t^* = \frac{D}{U}t,$$
$$p^* = \frac{\mu_d U}{D}p, \qquad \eta^* = \frac{\sigma}{\epsilon}\eta, \qquad \rho^* = \rho_d\lambda_1, \qquad \mu^* = \mu_d\lambda_2,$$
$$\beta \sim \frac{\sigma}{\epsilon}, \qquad \alpha \sim \sigma\epsilon. \tag{2.27 a, b, c, d, e, f, g, h, i, j, k}$$

After non-dimensionalization, we rewrite the governing equations in their non-dimensional forms:

$$\lambda_1 Re\left(\frac{\partial u}{\partial t} + u\frac{\partial u}{\partial r} + w\frac{\partial u}{\partial z}\right) = -\frac{\partial p}{\partial r} + \frac{1}{r}\frac{\partial}{\partial r}\left(r2\lambda_2\frac{\partial u}{\partial r}\right) + \frac{\partial}{\partial z}\left(\lambda_2\left(\frac{\partial u}{\partial z} + \frac{\partial w}{\partial r}\right)\right) - \frac{2\lambda_2 u}{r^2} + \frac{1}{CnCa}\eta\frac{\partial \phi}{\partial r}, \tag{2.28}$$

$$\lambda_1 Re\left(\frac{\partial w}{\partial t} + u\frac{\partial w}{\partial r} + w\frac{\partial w}{\partial z}\right) = -\frac{\partial p}{\partial z} + \frac{1}{r}\frac{\partial}{\partial r}\left(r\lambda_2\left(\frac{\partial u}{\partial z} + \frac{\partial w}{\partial r}\right)\right) + \frac{\partial}{\partial z}\left(2\lambda_2\frac{\partial w}{\partial z}\right) + \frac{1}{CnCa}\eta\frac{\partial \phi}{\partial z}, \tag{2.29}$$

$$\frac{\partial u}{\partial r} + \frac{u}{r} + \frac{\partial w}{\partial z} = 0, \tag{2.30}$$

$$\frac{\partial \phi}{\partial t} + u\frac{\partial \phi}{\partial r} + w\frac{\partial \phi}{\partial z} = \frac{1}{Pe}\left(\frac{1}{r}\frac{\partial}{\partial r}\left(r\frac{\partial \eta}{\partial r}\right) + \frac{\partial^2 \eta}{\partial z^2}\right), \tag{2.31}$$

$$\eta = -\phi + \phi^3 - Cn^2\left(\frac{1}{r}\frac{\partial}{\partial r}\left(r\frac{\partial \phi}{\partial r}\right) + \frac{\partial^2 \phi}{\partial z^2}\right). \tag{2.32}$$

The non-dimensional and linearly interpolated density and viscosity contrasts in (2.28) and (2.29) are

$$\lambda_1 = \frac{1+\phi+\rho(1-\phi)}{2}, \tag{2.33}$$

$$\lambda_2 = \frac{1+\phi+\mu(1-\phi)}{2}. \tag{2.34}$$

The dimensionless groups appearing in the non-dimensional equations are

$$Re = \frac{\rho_d U D}{\mu_d}, \qquad Cn = \frac{\epsilon}{D}, \qquad Ca = \frac{\mu_d U}{\sigma} = \frac{We}{Re},$$
$$We = \frac{\rho_d U^2 D}{\sigma}, \qquad Pe = \frac{U\epsilon D}{M\sigma}, \qquad \rho = \frac{\rho_a}{\rho_d}, \qquad \mu = \frac{\mu_a}{\mu_d}. \tag{2.35 a, b, c, d, e, f, g}$$

Re is the Reynolds number that relates the inertial forces in a fluid flow to the viscous forces. Cn is Cahn number that relates ratio of the diffuse interface width to the characteristic length scale. Ca is Capillary number that relates the viscous forces in a fluid to the surface tension forces. We is the Weber number defined as the ratio of inertial forces to surface tension forces. Pe is the Peclet number and it means advection to the rate of diffusion. The ρ and μ are the ratio of density and viscosity of ambient fluid to droplet respectively.

We, now, move to the next chapter in which we explain the numerical technique to integrate the model problem.

Chapter 3

Numerical Method

We integrate our model equations using Finite Element Method with quadratic unstructured triangular elements. We first obtain our weak formulation. To do so we multiply the set of equations with a weight function and integrate over the domain Ω where the coordinates satisfy $0 \leq r \leq 2.5, \quad 0 \leq z \leq 2.5$ and weaken the differentiability requirement. The test functions and approximations of the solution variables are picked from the same Hilbert-Sobolov $H_1(\Omega)$ space as requirement of the Galerkin approximation technique.

The unknown solution variables are u, w, p, ϕ, λ_1 and λ_2. The weights we multiply $r-$ momentum, $z-$momentum, continuity, Cahn-Hilliard and chemical potential equations are $\bar{u},\ \bar{w},\ \bar{p},\ \bar{\phi},\ \bar{\eta}$ respectively. Below we give the corresponding integral equations.

Before jumping into algebra, equations (2.28) and (2.29) can be written as

$$\begin{aligned} \lambda_1 Re\frac{\partial u}{\partial t} + \lambda_1 Re\, u\frac{\partial u}{\partial r} + \lambda_1 Re\, w\frac{\partial u}{\partial z} &= -\frac{\partial p}{\partial r} + \frac{2\lambda_2}{r}\frac{\partial u}{\partial r} \\ +2\frac{\partial \lambda_2}{\partial r}\frac{\partial u}{\partial r} + 2\mu\frac{\partial^2 u}{\partial r^2} + \frac{\partial \lambda_2}{\partial z}\frac{\partial u}{\partial z} + \mu\frac{\partial^2 u}{\partial z^2} + \frac{\partial \lambda_2}{\partial z}\frac{\partial w}{\partial r} & \\ +\lambda_2\frac{\partial^2 w}{\partial z \partial r} - \frac{2\lambda_2 u}{r^2} + \frac{1}{Cn\, Ca}\eta\frac{\partial \phi}{\partial r}, & \end{aligned} \tag{3.1}$$

$$\lambda_1 Re\frac{\partial w}{\partial t}+\lambda_1 Re\, u\frac{\partial w}{\partial r}+\lambda_1 Re\, w\frac{\partial w}{\partial z}=-\frac{\partial p}{\partial r}+\frac{\lambda_2}{r}\frac{\partial u}{\partial z}$$
$$+\frac{\partial \lambda_2}{\partial r}\frac{\partial u}{\partial z}+\mu\frac{\partial^2 u}{\partial r\partial z}+\frac{\lambda_2}{r}\frac{\partial w}{\partial r} \qquad (3.2)$$
$$+\frac{\partial \lambda_2}{\partial r}\frac{\partial w}{\partial r}+\lambda_2\frac{\partial^2 w}{\partial r^2}+2\frac{\partial \lambda_2}{\partial z}\frac{\partial w}{\partial z}+2\lambda_2\frac{\partial^2 w}{\partial z^2}+\frac{1}{Cn\,Ca}\eta\frac{\partial \phi}{\partial z}.$$

The equations (3.1) and (3.2) still need an approach to ease for weakening process. The terms with prefactor two are separated one by one then regrouped with other similar terms too appear as clusters shown below, first, for equation (3.1)

$$\lambda_1 Re\frac{\partial u}{\partial t}+\lambda_1 Re\, u\frac{\partial u}{\partial r}+\lambda_1 Re\, w\frac{\partial u}{\partial z}=-\frac{\partial p}{\partial r}$$
$$+\lambda_2\left(\frac{\partial^2 u}{\partial r^2}+\frac{1}{r}\frac{\partial u}{\partial r}+\frac{\partial^2 u}{\partial z^2}\right)+\lambda_2\left(\frac{\partial^2 u}{\partial r^2}+\frac{1}{r}\frac{\partial u}{\partial r}-\frac{u}{r^2}+\frac{\partial w}{\partial z\partial r}\right) \qquad (3.3)$$
$$+2\frac{\partial \lambda_2}{\partial r}\frac{\partial u}{\partial r}+\frac{\partial \lambda_2}{\partial z}\frac{\partial u}{\partial z}+\frac{\partial \lambda_2}{\partial z}\frac{\partial w}{\partial r}-\frac{\lambda_2 u}{r^2}+\frac{1}{Cn\,Ca}\eta\frac{\partial \phi}{\partial r},$$

$$\lambda_1 Re\frac{\partial u}{\partial t}+\lambda_1 Re\, u\frac{\partial u}{\partial r}+\lambda_1 Re\, w\frac{\partial u}{\partial z}=-\frac{\partial p}{\partial r}$$
$$+\lambda_2\nabla^2\mathbf{u}+\lambda_2\left(\frac{\partial}{\partial r}\left(\frac{\partial u}{\partial r}+\frac{u}{r}+\frac{\partial w}{\partial z}\right)\right) \qquad (3.4)$$
$$+2\frac{\partial \lambda_2}{\partial r}\frac{\partial u}{\partial r}+\frac{\partial \lambda_2}{\partial z}\frac{\partial u}{\partial z}+\frac{\partial \lambda_2}{\partial z}\frac{\partial w}{\partial r}-\frac{\lambda_2 u}{r^2}+\frac{1}{Cn\,Ca}\eta\frac{\partial \phi}{\partial r},$$

$$\lambda_1 Re\frac{\partial u}{\partial t}+\lambda_1 Re\, u\frac{\partial u}{\partial r}+\lambda_1 Re\, w\frac{\partial u}{\partial z}=-\frac{\partial p}{\partial r}$$
$$+\lambda_2\nabla^2\mathbf{u}+\lambda_2\nabla(\nabla\cdot\mathbf{u}) \tag{3.5}$$
$$+2\frac{\partial\lambda_2}{\partial r}\frac{\partial u}{\partial r}+\frac{\partial\lambda_2}{\partial z}\frac{\partial u}{\partial z}+\frac{\partial\lambda_2}{\partial z}\frac{\partial w}{\partial r}-\frac{\lambda_2 u}{r^2}+\frac{1}{Cn\,Ca}\eta\frac{\partial\phi}{\partial r}.$$

We knew that $\nabla\cdot\mathbf{u}=0$, then

$$\lambda_1 Re\frac{\partial u}{\partial t}+\lambda_1 Re\, u\frac{\partial u}{\partial r}+\lambda_1 Re\, w\frac{\partial u}{\partial z}=-\frac{\partial p}{\partial r}$$
$$+\lambda_2\nabla^2\mathbf{u}-\frac{\lambda_2 u}{r^2}+2\frac{\partial\lambda_2}{\partial r}\frac{\partial u}{\partial r}+\frac{\partial\lambda_2}{\partial z}\frac{\partial u}{\partial z}+\frac{\partial\lambda_2}{\partial z}\frac{\partial w}{\partial r}+\frac{1}{Cn\,Ca}\eta\frac{\partial\phi}{\partial r}. \tag{3.6}$$

We follow the same steps for equation (3.2) and this results with

$$\lambda_1 Re\frac{\partial w}{\partial t}+\lambda_1 Re\, u\frac{\partial w}{\partial r}+\lambda_1 Re\, w\frac{\partial w}{\partial z}=-\frac{\partial p}{\partial r}$$
$$+\lambda_2\nabla^2\mathbf{w}+\frac{\partial\lambda_2}{\partial r}\frac{\partial u}{\partial z}+\frac{\partial\lambda_2}{\partial r}\frac{\partial w}{\partial r}+2\frac{\partial\lambda_2}{\partial z}\frac{\partial w}{\partial z}+\frac{1}{Cn\,Ca}\eta\frac{\partial\phi}{\partial z}. \tag{3.7}$$

Last two governing equations are regrouped for same purpose and (2.30), (2.31) and (2.32) are,

$$\frac{\partial u}{\partial r}+\frac{u}{r}+\frac{\partial w}{\partial z}=0, \tag{3.8}$$

$$\frac{\partial\phi}{\partial t}+u\frac{\partial\phi}{\partial r}+w\frac{\partial\phi}{\partial z}=\frac{1}{Pe}\nabla^2\eta, \tag{3.9}$$

$$\eta=-\phi+\phi^3-Cn^2\nabla^2\phi. \tag{3.10}$$

Now the set of equations (3.6), (3.7), (3.8), (3.9) and (3.10) are multiplied with corresponding test functions and integrated over the domain as

$$\lambda_1 Re \int_\Omega \frac{\partial u}{\partial t}\bar{u}\,\mathrm{d}\Omega + \lambda_1 Re \int_\Omega u\frac{\partial u}{\partial r}\bar{u}\,\mathrm{d}\Omega + \lambda_1 Re \int_\Omega w\frac{\partial u}{\partial z}\bar{u}\,\mathrm{d}\Omega =$$
$$-\int_\Omega \frac{\partial p}{\partial r}\bar{u}\,\mathrm{d}\Omega + \int_\Omega \lambda_2 \nabla^2 \mathbf{u}\bar{u}\,\mathrm{d}\Omega + 2\int_\Omega \frac{\partial \lambda_2}{\partial r}\frac{\partial u}{\partial r}\bar{u}\,\mathrm{d}\Omega$$
$$+\int_\Omega \frac{\partial \lambda_2}{\partial z}\frac{\partial u}{\partial z}\bar{u}\,\mathrm{d}\Omega + \int_\Omega \frac{\partial \lambda_2}{\partial z}\frac{\partial w}{\partial r}\bar{u}\,\mathrm{d}\Omega - \int_\Omega \frac{\lambda_2 u}{r^2}\bar{u}\,\mathrm{d}\Omega \tag{3.11}$$
$$+\frac{1}{Cn\,Ca}\int_\Omega \eta\frac{\partial \phi}{\partial r}\bar{u}\,\mathrm{d}\Omega,$$

$$\lambda_1 Re \int_\Omega \frac{\partial w}{\partial t}\bar{w}\,\mathrm{d}\Omega + \lambda_1 Re \int_\Omega u\frac{\partial w}{\partial r}\bar{w}\,\mathrm{d}\Omega + \lambda_1 Re \int_\Omega w\frac{\partial w}{\partial z}\bar{w}\,\mathrm{d}\Omega =$$
$$-\int_\Omega \frac{\partial p}{\partial r}\bar{w}\,\mathrm{d}\Omega + \int_\Omega \lambda_2 \nabla^2 \mathbf{w}\bar{w}\,\mathrm{d}\Omega + \int_\Omega \frac{\partial \lambda_2}{\partial r}\frac{\partial u}{\partial z}\bar{w}\,\mathrm{d}\Omega \tag{3.12}$$
$$+\int_\Omega \frac{\partial \lambda_2}{\partial r}\frac{\partial w}{\partial r}\bar{w}\,\mathrm{d}\Omega + 2\int_\Omega \frac{\partial \lambda_2}{\partial z}\frac{\partial w}{\partial z}\bar{w}\,\mathrm{d}\Omega + \frac{1}{Cn\,Ca}\int_\Omega \eta\frac{\partial \phi}{\partial z}\bar{w}\,\mathrm{d}\Omega,$$

$$\int_\Omega \frac{\partial u}{\partial r}\bar{p}\,\mathrm{d}\Omega + \int_\Omega \frac{u}{r}\bar{p}\,\mathrm{d}\Omega + \int_\Omega \frac{\partial w}{\partial z}\bar{p}\,\mathrm{d}\Omega = 0, \tag{3.13}$$

$$\int_\Omega \frac{\partial \phi}{\partial t}\bar{\phi}\,\mathrm{d}\Omega + \int_\Omega u\frac{\partial \phi}{\partial r}\bar{\phi}\,\mathrm{d}\Omega + \int_\Omega w\frac{\partial \phi}{\partial z}\bar{\phi}\,\mathrm{d}\Omega = \frac{1}{Pe}\int_\Omega \nabla^2\eta\,\bar{\phi}\,\mathrm{d}\Omega, \tag{3.14}$$

$$\int_\Omega \eta\bar{\eta}\,\mathrm{d}\Omega = -\int_\Omega \phi\,\bar{\eta}\,\mathrm{d}\Omega + \int_\Omega \phi^3\bar{\eta}\,\mathrm{d}\Omega - Cn^2\int_\Omega \nabla^2\phi\bar{\eta}\,\mathrm{d}\Omega. \tag{3.15}$$

To weaken the differentiability requirements, we modify the equations by taking the weight functions into the second order derivatives and subtracting the extra terms. We, then, perform integrations, if possible, to convert the area integrals to line integrals using divergence theorem and pick the weight functions to be zero at any Dirichlet boundary condition. Also, unknowns are separated from the rest of the terms. We rewrite (3.11) as

$$
\begin{aligned}
&Re\int_\Omega \lambda_1 \frac{\partial u}{\partial t}\bar{u}\,\mathrm{d}\Omega + Re\int_\Omega \lambda_1 u\frac{\partial u}{\partial r}\bar{u}\,\mathrm{d}\Omega + Re\int_\Omega \lambda_1 w\frac{\partial u}{\partial z}\bar{u}\,\mathrm{d}\Omega = \\
&-\int_\Omega \frac{\partial p}{\partial r}\bar{u}\,\mathrm{d}\Omega + \int_\Omega \nabla(\lambda_2 \nabla \mathbf{u}\bar{u})\,\mathrm{d}\Omega \\
&-\int_\Omega \nabla\lambda_2\cdot\nabla\mathbf{u}\bar{u}\,\mathrm{d}\Omega - \int_\Omega \lambda_2\nabla\mathbf{u}\cdot\nabla\bar{u}\,\mathrm{d}\Omega \\
&+2\int_\Omega \frac{\partial\lambda_2}{\partial r}\frac{\partial u}{\partial r}\bar{u}\,\mathrm{d}\Omega + \int_\Omega \frac{\partial\lambda_2}{\partial z}\frac{\partial u}{\partial z}\bar{u}\,\mathrm{d}\Omega + \int_\Omega \frac{\partial\lambda_2}{\partial z}\frac{\partial w}{\partial r}\bar{u}\,\mathrm{d}\Omega \\
&-\int_\Omega \frac{\lambda_2 u}{r^2}\bar{u}\,\mathrm{d}\Omega + \frac{1}{Cn\,Ca}\int_\Omega \eta\frac{\partial\phi}{\partial r}\bar{u}\,\mathrm{d}\Omega,
\end{aligned}
\tag{3.16}
$$

$$
\begin{aligned}
&Re\int_\Omega \lambda_1 \frac{\partial u}{\partial t}\bar{u}\,\mathrm{d}\Omega + Re\int_\Omega \lambda_1 u\frac{\partial u}{\partial r}\bar{u}\,\mathrm{d}\Omega + Re\int_\Omega \lambda_1 w\frac{\partial u}{\partial z}\bar{u}\,\mathrm{d}\Omega = \\
&-\int_\Omega \frac{\partial p}{\partial r}\bar{u}\,\mathrm{d}\Omega - \int_\Omega \lambda_2\frac{\partial u}{\partial r}\frac{\partial\bar{u}}{\partial r}\,\mathrm{d}\Omega - \int_\Omega \lambda_2\frac{\partial u}{\partial z}\frac{\partial\bar{u}}{\partial r}\,\mathrm{d}\Omega - \int_\Omega \frac{\lambda_2 u}{r^2}\bar{u}\,\mathrm{d}\Omega \\
&+\int_\Omega \frac{\partial\lambda_2}{\partial r}\frac{\partial u}{\partial r}\bar{u}\,\mathrm{d}\Omega + \int_\Omega \frac{\partial\lambda_2}{\partial z}\frac{\partial w}{\partial r}\bar{u}\,\mathrm{d}\Omega + \frac{1}{Cn\,Ca}\int_\Omega \eta\frac{\partial\phi}{\partial r}\bar{u}\,\mathrm{d}\Omega.
\end{aligned}
\tag{3.17}
$$

and (3.12) as

$$
\begin{aligned}
&Re\int_\Omega \lambda_1 \frac{\partial w}{\partial t}\bar{w}\,\mathrm{d}\Omega + Re\int_\Omega \lambda_1 u\frac{\partial w}{\partial r}\bar{w}\,\mathrm{d}\Omega + Re\int_\Omega \lambda_1 w\frac{\partial w}{\partial z}\bar{w}\,\mathrm{d}\Omega = \\
&-\int_\Omega \frac{\partial p}{\partial r}\bar{w}\mathrm{d}\Omega + \int_\Omega \nabla(\lambda_2\nabla\mathbf{w}\bar{w})\mathrm{d}\Omega - \int_\Omega \nabla\lambda_2\cdot\nabla\mathbf{w}\bar{w}\mathrm{d}\Omega \\
&-\int_\Omega \lambda_2\nabla\mathbf{w}\cdot\nabla\bar{w}\mathrm{d}\Omega + \int_\Omega \frac{\partial\lambda_2}{\partial r}\frac{\partial u}{\partial z}\bar{w}\,\mathrm{d}\Omega + \int_\Omega \frac{\partial\lambda_2}{\partial r}\frac{\partial w}{\partial r}\bar{w}\mathrm{d}\Omega \\
&+2\int_\Omega \frac{\partial\lambda_2}{\partial z}\frac{\partial w}{\partial z}\bar{w}\,\mathrm{d}\Omega + \frac{1}{Cn\,Ca}\int_\Omega \eta\frac{\partial\phi}{\partial z}\bar{w}\mathrm{d}\Omega,
\end{aligned}
\tag{3.18}
$$

$$Re\int_{\Omega}\lambda_1\frac{\partial w}{\partial t}\bar{w}\,\mathrm{d}\Omega + Re\int_{\Omega}\lambda_1 u\frac{\partial w}{\partial r}\bar{w}\,\mathrm{d}\Omega + Re\int_{\Omega}\lambda_1 w\frac{\partial w}{\partial z}\bar{w}\mathrm{d}\Omega =$$
$$-\int_{\Omega}\frac{\partial p}{\partial r}\bar{w}\,\mathrm{d}\Omega - \int_{\Omega}\lambda_2\frac{\partial w}{\partial r}\frac{\partial \bar{w}}{\partial r}\,\mathrm{d}\Omega - \int_{\Omega}\lambda_2\frac{\partial w}{\partial z}\frac{\partial \bar{w}}{\partial z}\mathrm{d}\Omega \tag{3.19}$$
$$+\int_{\Omega}\frac{\partial\lambda_2}{\partial z}\frac{\partial w}{\partial z}\bar{w}\,\mathrm{d}\Omega + \int_{\Omega}\frac{\partial\lambda_2}{\partial r}\frac{\partial u}{\partial z}\bar{w}\,\mathrm{d}\Omega + \frac{1}{Cn\,Ca}\int_{\Omega}\eta\frac{\partial\phi}{\partial z}\bar{w}\,\mathrm{d}\Omega.$$

Continuity does not change, the Cahn-Hilliard becomes

$$\int_{\Omega}\frac{\partial\phi}{\partial t}\bar{\phi}\,\mathrm{d}\Omega + \int_{\Omega}u\frac{\partial\phi}{\partial r}\bar{\phi}\,\mathrm{d}\Omega + \int_{\Omega}w\frac{\partial\phi}{\partial z}\bar{\phi}\,\mathrm{d}\Omega =$$
$$\frac{1}{Pe}\int_{\Omega}\nabla(\nabla\eta\bar{\phi})\,\mathrm{d}\Omega - \frac{1}{Pe}\int_{\Omega}\nabla\eta\nabla\bar{\phi}\,\mathrm{d}\Omega, \tag{3.20}$$

$$\int_{\Omega}\frac{\partial\phi}{\partial t}\bar{\phi}\,\mathrm{d}\Omega + \int_{\Omega}u\frac{\partial\phi}{\partial r}\bar{\phi}\,\mathrm{d}\Omega + \int_{\Omega}w\frac{\partial\phi}{\partial z}\bar{\phi}\,\mathrm{d}\Omega =$$
$$\frac{1}{Pe}\int_{\Omega}\frac{\partial\eta}{\partial r}\frac{\partial\bar{\phi}}{\partial r}\,\mathrm{d}\Omega - \frac{1}{Pe}\int_{\Omega}\frac{\partial\eta}{\partial z}\frac{\partial\bar{\phi}}{\partial z}\,\mathrm{d}\Omega \tag{3.21}$$

and the chemical potential is written as,

$$\int_{\Omega}\eta\bar{\eta}\,\mathrm{d}\Omega = -\int_{\Omega}\phi\,\bar{\eta}\,\mathrm{d}\Omega + \int_{\Omega}\phi^3\bar{\eta}\,\mathrm{d}\Omega$$
$$-Cn^2\int_{\Omega}\nabla(\nabla\phi\bar{\eta})\,\mathrm{d}\Omega + Cn^2\int_{\Omega}\nabla\phi\nabla\bar{\eta}\,\mathrm{d}\Omega. \tag{3.22}$$

The volume integral, third term in (3.22) right hand side, is converted into surface integral with the use of divergence theorem which is the only non-zero surface integral with which we apply the wetting boundary condition. We rewrite (3.22) as

$$\int_{\Omega}\eta\bar{\eta}\,\mathrm{d}\Omega = -\int_{\Omega}\phi\,\bar{\eta}\,\mathrm{d}\Omega + \int_{\Omega}\phi^3\bar{\eta}\,\mathrm{d}\Omega \tag{3.23}$$

$$+Cn^2 \int_\Omega \frac{\partial \phi}{\partial r}\frac{\partial \bar{\eta}}{\partial r}\,\mathrm{d}\Omega + Cn^2 \int_\Omega \frac{\partial \phi}{\partial z}\frac{\partial \bar{\eta}}{\partial z}\,\mathrm{d}\Omega$$

$$-Cn^2 \oint_{\partial\Omega_b} (n \cdot \nabla\phi)\bar{\eta}\,\mathrm{d}\partial\Omega_b.$$

Because the model problem is axisymmetric, we perform the azimuthal integration analytically as there is no dependence on θ. In this case, we define the differential domain as $d\Omega = 2\pi r\, drdz$. As 2π appears everywhere, we cancel it and rewrite the final form of the governing set of equations.

We first map the physical finite elements to a master element in r − s domain and perform all the integrations in this domain.

3.1 Space and Time Discretizations

For the finite element solution of the equations, the domain and the solution variables are discretized using $P2 - P1$ triangular elements. A representative domain we studied on given in Figure 3.1. The values of velocities, phase field and chemical potential are represented by the nodal points one to six, and are interpolated using quadratic polynomials. Likewise, the pressure is determined by the three corner nodal values one to three and is interpolated using a linear polynomial.

The two-dimensional cylindrical coordinate system (with the advantage of it one can say semi-three-dimensional coordinate system) is transformed into natural coordinates within the Gauss quadrature rule.

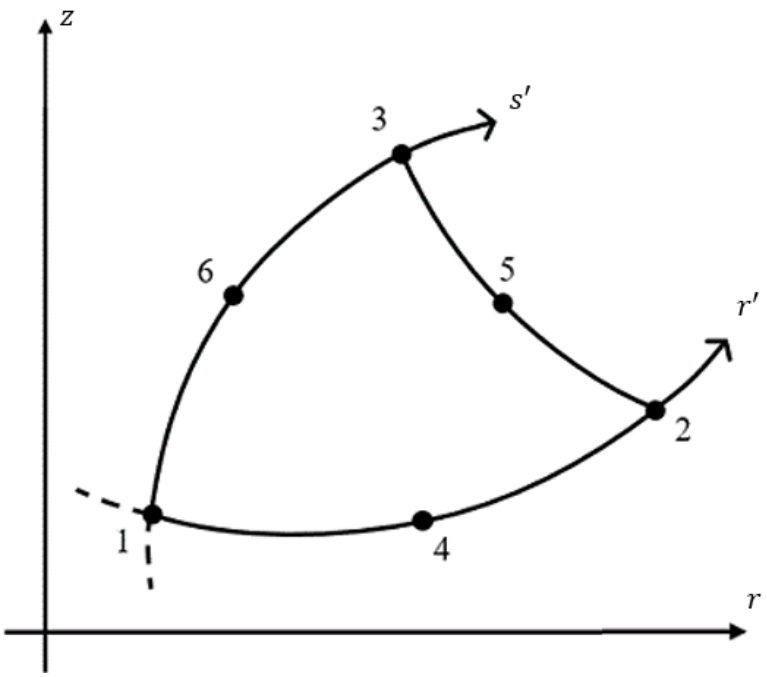

Figure 3.1: Master element and nodal points in the isoperimetric plane.

For the quadratic velocity components, ϕ and η, we use the following six interpolation functions

$$\begin{gathered}
{\varphi_1}^q(r',s') = 1 - 3r' - 3s' + 2r'^2 + 4r's' + 2s'^2, \\
{\varphi_2}^q(r',s') = -r' + 2r'^2, \\
{\varphi_3}^q(r',s') = -s' + 2s'^2, \\
{\varphi_4}^q(r',s') = 4r' - 4r'^2 - 4r's', \\
{\varphi_5}^q(r',s') = 4r's', \\
{\varphi_6}^q(r',s') = 4s' - 4r's' - 4s'^2.
\end{gathered} \qquad \text{(3.24 a, b, c, d, e, f)}$$

and for the pressure, the three following linear interpolation functions are used

$$\begin{gathered}
{\varphi_1}^l(r',s') = 1 - r' - s', \\
{\varphi_2}^l(r',s') = r', \\
{\varphi_3}^l(r',s') = s'.
\end{gathered} \qquad \text{(3.25 a, b, c)}$$

These functions are defined as piecewise continuous polynomials over sub elements. Derivatives with respect to r and s are also needed for the solver.

To map $r-z$ domain to $r'-s'$ domain, we approximate the $r-z$ coordinates using quadratic shape functions:

$$r(r',s') = \sum_{i=1}^{6} r_i \varphi_i{}^q, \tag{3.26}$$

$$z(r',s') = \sum_{i=1}^{6} z_i \varphi_i{}^q. \tag{3.27}$$

In (3.26) and (3.27), r_i and z_i are the coordinates of the nodal points in the physical domain. To perform integration in the $r'-s'$ domain, we need to express the mapping of derivatives from the $r-z$ plane to the isoperimetric plane using the Jacobian provided by

$$J = \begin{bmatrix} \dfrac{\partial r}{\partial r'} & \dfrac{\partial z}{\partial r'} \\ \dfrac{\partial r}{\partial s'} & \dfrac{\partial z}{\partial s'} \end{bmatrix}. \tag{3.28}$$

Using (3.28), the derivative operators can be represented as

$$\begin{bmatrix} \dfrac{\partial}{\partial r} \\ \dfrac{\partial}{\partial z} \end{bmatrix} = J^{-1} \begin{bmatrix} \dfrac{\partial}{\partial r'} \\ \dfrac{\partial}{\partial s'} \end{bmatrix}. \tag{3.29}$$

We use Gauss quadrature to compute the integrals which are calculated over triangles by applying the 7-point Gauss integration rule. In theory, evaluating the matrices accurately is only possible when a high enough order is used, otherwise, the problem solution may not be possible. The highest order (p) polynomial in the integrations is four so minimum number of Gauss Points should be calculated from equation of $p = 2n-1$ where n is number of Gauss Points, therefore the integrations are exact throughout the numerical method. Because as shown in equation, required number of Gauss Points is three and we use seven.

We need to solve a linear system for each time step and implicit method is generally stable and we can use higher Δt's which is computationally cheaper. The unsteady

term is easily approximated by applying a first order backward differentiation formula (BDF) scheme

$$\frac{\partial f}{\partial t} = \frac{f^{n+1} - f^{n}}{\Delta t}. \tag{3.30}$$

For better numerical treatment, we open the term λ_1 that multiplies with u_t and w_t. After putting this into system of equations (3.17), (3.19), (3.20), (3.21) and (3.23) become

$$\begin{aligned}
&Re\int_{\Omega}\lambda_1^{n+1}u^{n+1}\bar{u}d\Omega + \Delta tRe\int_{\Omega}\lambda_1^{n+1}u^{n+1}\frac{\partial u^{n+1}}{\partial r}\bar{u}d\Omega \\
&+\Delta tRe\int_{\Omega}\lambda_1^{n+1}w^{n+1}\frac{\partial u^{n+1}}{\partial z}\bar{u}d\Omega = -\Delta t\int_{\Omega}\frac{\partial p^{n+1}}{\partial r}\bar{u}d\Omega \\
&-\Delta t\int_{\Omega}\lambda_2^{n+1}\frac{\partial u^{n+1}}{\partial r}\frac{\partial \bar{u}}{\partial r}d\Omega - \Delta t\int_{\Omega}\lambda_2^{n+1}\frac{\partial u^{n+1}}{\partial z}\frac{\partial \bar{u}}{\partial z}d\Omega \\
&-\Delta t\int_{\Omega}\frac{\lambda_2^{n+1}u^{n+1}\bar{u}}{\partial r^2}d\Omega + \Delta t\int_{\Omega}\frac{\partial\lambda_2^{n+1}}{\partial r}\frac{\partial u^{n+1}}{\partial r}\bar{u}d\Omega \\
&+\Delta t\int_{\Omega}\frac{\partial\lambda_2^{n+1}}{\partial z}\frac{\partial u^{n+1}}{\partial r}\bar{u}d\Omega + \frac{\Delta t}{Cn\ Ca}\int_{\Omega}\eta^{n+1}\frac{\partial\phi^{n+1}}{\partial r}\bar{u}d\Omega \\
&+\frac{Re(1-\rho)}{2}\int_{\Omega}\phi^{n+1}u^{n}\bar{u}d\Omega + \frac{Re(1+\rho)}{2}\int_{\Omega}u^{n}\bar{u}d\Omega
\end{aligned} \tag{3.31}$$

$$\begin{aligned}
&Re\int_{\Omega}\lambda_1^{n+1}w^{n+1}\bar{w}d\Omega + \Delta tRe\int_{\Omega}\lambda_1^{n+1}u^{n+1}\frac{\partial w^{n+1}}{\partial r}\bar{w}d\Omega \\
&+\Delta tRe\int_{\Omega}\lambda_1^{n+1}w^{n+1}\frac{\partial w^{n+1}}{\partial z}\bar{w}d\Omega = -\Delta t\int_{\Omega}\frac{\partial p^{n+1}}{\partial z}\bar{w}d\Omega \\
&-\Delta t\int_{\Omega}\lambda_2^{n+1}\frac{\partial w^{n+1}}{\partial r}\frac{\partial \bar{w}}{\partial r}d\Omega - \Delta t\int_{\Omega}\lambda_2^{n+1}\frac{\partial w^{n+1}}{\partial z}\frac{\partial \bar{w}}{\partial z}d\Omega
\end{aligned} \tag{3.32}$$

$$+\Delta t\int_{\Omega}\frac{\partial\lambda_2^{n+1}}{\partial z}\frac{\partial w^{n+1}}{\partial z}\bar{w}d\Omega+\Delta t\int_{\Omega}\frac{\partial\lambda_2^{n+1}}{\partial r}\frac{\partial u^{n+1}}{\partial z}\bar{w}d\Omega$$

$$+\frac{\Delta t}{Cn\,Ca}\int_{\Omega}\eta^{n+1}\frac{\partial\phi^{n+1}}{\partial z}\bar{u}d\Omega+\frac{Re(1-\rho)}{2}\int_{\Omega}\phi^{n+1}w^{n}\bar{w}d\Omega$$

$$+\frac{Re(1+\rho)}{2}\int_{\Omega}w^{n}\bar{w}d\Omega-\Delta t\frac{Bo}{Ca}\int_{\Omega}\bar{w}d\Omega$$

$$\int_{\Omega}\frac{\partial u^{n+1}}{\partial r}\bar{p}d\Omega+\int_{\Omega}\frac{u^{n+1}}{r}\bar{p}d\Omega+\int_{\Omega}\frac{\partial w^{n+1}}{\partial z}\bar{p}d\Omega\ =0 \tag{3.33}$$

$$\begin{aligned}&\int_{\Omega}\phi^{n+1}\bar{\phi}d\Omega+\Delta t\int_{\Omega}u^{n+1}\frac{\partial\phi^{n+1}}{\partial r}\bar{\phi}d\Omega+\Delta t\int_{\Omega}w^{n+1}\frac{\partial\phi^{n+1}}{\partial z}\bar{\phi}d\Omega\\&=-\frac{\Delta t}{Pe}\int_{\Omega}\frac{\partial\eta^{n+1}}{\partial r}\frac{\partial\bar{\phi}}{\partial r}d\Omega-\frac{\Delta t}{Pe}\int_{\Omega}\frac{\partial\eta^{n+1}}{\partial z}\frac{\partial\bar{\phi}}{\partial z}d\Omega+\int_{\Omega}\phi^{n}\bar{\phi}d\Omega\end{aligned} \tag{3.34}$$

$$\begin{aligned}&\int_{\Omega}\eta^{n+1}\bar{\eta}d\Omega=-\int_{\Omega}\phi^{n+1}\bar{\eta}d\Omega\int_{\Omega}{\phi^{n+1}}^{3}\bar{\eta}d\Omega\\&+Cn^2\int_{\Omega}\frac{\partial\phi^{n+1}}{\partial r}\frac{\partial\bar{\eta}}{\partial r}d\Omega+Cn^2\int_{\Omega}\frac{\partial\phi^{n+1}}{\partial z}\frac{\partial\bar{\eta}}{\partial z}d\Omega\\&-Cn^2\oint_{\partial\Omega_b}(\boldsymbol{n}\cdot\nabla\phi)\,\bar{\eta}d\partial\Omega_b\end{aligned} \tag{3.35}$$

We next define finite element space approximations of u^{n+1}, w^{n+1}, p^{n+1}, ϕ^{n+1}, η^{n+1}, λ_1^{n+1}, λ_2^{n+1}, u^n, w^n, ϕ^n, $\bar{u}$, $\bar{w}$, $\bar{p}$, $\bar{\phi}$, $\bar{\eta}$, $\bar{\lambda}_1$, $\bar{\lambda}_2$. All the interpolation functions, except the pressure, and their weight functions are piece-wise quadratic while the pressure terms are linear in space defined over triangular elements in the isoperimetric plane.

$$u^{n+1}=\sum_{j=1}^{6}u_j^{n+1}\varphi_j^q,\ w^{n+1}=\sum_{j=1}^{6}w_j^{n+1}\varphi_j^q, p^{n+1}=\sum_{j=1}^{3}p_j^{n+1}\varphi_j^l,$$

$$\phi^{n+1}=\sum_{j=1}^{6}\phi_j^{n+1}\varphi_j^q,\ \eta^{n+1}=\sum_{j=1}^{6}\eta_j^{n+1}\varphi_j^q,\ \lambda_1^{n+1}=\sum_{j=1}^{6}{\lambda_1}_j^{n+1}\varphi_j^q,$$

$$\lambda_2^{n+1}=\sum_{j=1}^{6}{\lambda_2}_j^{n+1}\varphi_j^q,\ u^n=\sum_{j=1}^{6}u_j^n\varphi_j^q,\ w^n=\sum_{j=1}^{6}w_j^n\varphi_j^q, \qquad (3.36\ a, b, c, d, e, f, g, h, i, j, k, l, m, n, o)$$

$$\phi^n=\sum_{j=1}^{6}\phi_j^n\varphi_j^q,\ \bar{u}=\sum_{i=1}^{6}\bar{u}_i\varphi_i^q,\ \bar{w}=\sum_{i=1}^{6}\bar{w}_i\varphi_i^q,$$

$$\bar{p}=\sum_{i=1}^{3}\bar{p}_i\varphi_i^l,\ \bar{\phi}=\sum_{i=1}^{6}\bar{\phi}_i\varphi_i^q,\ \bar{\eta}=\sum_{i=1}^{6}\bar{\eta}_i\varphi_i^q.$$

The ${\varphi_j}^q$ and ${\varphi_j}^l$ are quadratic and linear interpolations; $u_j, w_j, p_j, \phi_j, \eta_j, {\lambda_1}_j$ and ${\lambda_2}_j$ are the nodal values. We substitute them back into the equations and use the fact that, the weak form is valid, for all $\bar{u}_i$, $\bar{w}_i, \bar{p}, \bar{\eta}_i$and $\bar{\phi}_i$. We take the summations out of integrals and define the system to be solved for the unknowns. All the knowns are collected at the right-hand side and the unknowns to left-hand side of the equation.

$$\sum_{i=1}^{6}\bar{u}_i\left[Re\sum_{j=1}^{6}u_j^{n+1}\underbrace{\left(\int_\Omega\left(\sum_{j=1}^{6}{\lambda_1}_j^{n+1}\varphi_j^q\right)\varphi_j^q\varphi_i^q\,d\Omega\right)}_{\mathrm{LU}_{ij}}\right.$$

$$+\Delta tRe\sum_{j=1}^{6}u_j^{n+1}\underbrace{\left(\int_\Omega\left(\sum_{j=1}^{6}{\lambda_1}_j^{n+1}\varphi_j^q\right)\left(\sum_{j=1}^{6}u_j^{n+1}\frac{\partial\varphi_j^q}{\partial r}\right)\varphi_j^q\varphi_i^q\,d\Omega\right)}_{\mathrm{LKNUR}_{ij}}$$

$$\left.+\Delta tRe\sum_{j=1}^{6}w_j^{n+1}\underbrace{\left(\int_\Omega\left(\sum_{j=1}^{6}{\lambda_1}_j^{n+1}\varphi_j^q\right)\left(\sum_{j=1}^{6}u_j^{n+1}\frac{\partial\varphi_j^q}{\partial z}\right)\varphi_j^q\varphi_i^q\,d\Omega\right)}_{\mathrm{LKNUZ}_{ij}}\right.$$

$$+\Delta t\sum_{j=1}^{3} p_j^{n+1}\underbrace{\left(\int_\Omega \frac{\partial \varphi_j^l}{\partial r}\varphi_i^q\, d\Omega\right)}_{\mathrm{PR}_{ij}}$$

$$+\Delta t\sum_{j=1}^{6} u_j^{n+1}\underbrace{\left(\int_\Omega\left(\sum_{j=1}^{6}{\lambda_2}_j^{n+1}\varphi_j^q\right)\frac{\partial \varphi_j^q}{\partial r}\frac{\partial \varphi_i^q}{\partial r}d\Omega\right)}_{\mathrm{LL}_{ij}}$$

$$+\Delta t\sum_{j=1}^{6} u_j^{n+1}\underbrace{\left(\int_\Omega\left(\sum_{j=1}^{6}{\lambda_2}_j^{n+1}\varphi_j^q\right)\frac{\partial \varphi_j^q}{\partial z}\frac{\partial \varphi_i^q}{\partial z}d\Omega\right)}_{\mathrm{LM}_{ij}}$$

$$+\Delta t\sum_{j=1}^{6} u_j^{n+1}\underbrace{\left(\int_\Omega\left(\sum_{j=1}^{6}{\lambda_2}_j^{n+1}\varphi_j^q\right)\frac{\varphi_j^q\varphi_i^q}{r^2}d\Omega\right)}_{\mathrm{LR2}_{ij}} \qquad (3.37)$$

$$-\Delta t\sum_{j=1}^{6} u_j^{n+1}\underbrace{\left(\int_\Omega\left(\sum_{j=1}^{6}{\lambda_2}_j^{n+1}\frac{\partial \varphi_j^q}{\partial r}\right)\frac{\partial \varphi_j^q}{\partial r}\varphi_i^q\, d\Omega\right)}_{\mathrm{DURR}_{ij}}$$

$$-\Delta t\sum_{j=1}^{6} w_j^{n+1}\underbrace{\left(\int_\Omega\left(\sum_{j=1}^{6}{\lambda_2}_j^{n+1}\frac{\partial \varphi_j^q}{\partial z}\right)\frac{\partial \varphi_j^q}{\partial r}\varphi_i^q\, d\Omega\right)}_{\mathrm{DWZR}_{ij}}$$

$$-\frac{\Delta t}{CnCa}\sum_{j=1}^{6}\eta_j^{n+1}\underbrace{\left(\int_\Omega\left(\sum_{j=1}^{6}\phi_j^{n+1}\frac{\partial \varphi_j^q}{\partial r}\right)\varphi_j^q\varphi_i^q\, d\Omega\right)}_{\mathrm{KNPHIR}_{ij}}$$

$$-\frac{Re(1-\rho)}{2}\sum_{j=1}^{6}\phi_j^{n+1}\underbrace{\left(\int_\Omega\left(\sum_{j=1}^{6}\mathrm{u}_j^n\varphi_j^q\right)\varphi_j^q\varphi_i^q\, d\Omega\right)}_{\mathrm{UU}_{ij}}$$

$$=\frac{Re(1+\rho)}{2}\sum_{j=1}^{6}\mathrm{u}_j^n\underbrace{\left(\int_\Omega\varphi_j^q\varphi_i^q\, d\Omega\right)}_{\mathrm{U}_{ij}}\Bigg]$$

$$\sum_{i=1}^{6}\overline{w}_i\Bigg[Re\sum_{j=1}^{6}w_j^{n+1}\underbrace{\left(\int_\Omega\left(\sum_{j=1}^{6}{\lambda_1}_j^{n+1}\varphi_j^q\right)\varphi_j^q\varphi_i^q\,d\Omega\right)}_{\mathrm{LU}_{ij}}$$

$$+\Delta tRe\sum_{j=1}^{6}u_j^{n+1}\underbrace{\left(\int_\Omega\left(\sum_{j=1}^{6}{\lambda_1}_j^{n+1}\varphi_j^q\right)\left(\sum_{j=1}^{6}u_j^{n+1}\frac{\partial\varphi_j^q}{\partial r}\right)\varphi_j^q\varphi_i^q\,d\Omega\right)}_{\mathrm{LKNWR}_{ij}}$$

$$+\Delta tRe\sum_{j=1}^{6}w_j^{n+1}\underbrace{\left(\int_\Omega\left(\sum_{j=1}^{6}{\lambda_1}_j^{n+1}\varphi_j^q\right)\left(\sum_{j=1}^{6}w_j^{n+1}\frac{\partial\varphi_j^q}{\partial z}\right)\varphi_j^q\varphi_i^q\,d\Omega\right)}_{\mathrm{LKNWZ}_{ij}}$$

$$+\Delta t\sum_{j=1}^{3}p_j^{n+1}\underbrace{\left(\int_\Omega\frac{\partial\varphi_j^l}{\partial z}\varphi_i^q\,d\Omega\right)}_{\mathrm{PZ}_{ij}}$$

$$+\Delta t\sum_{j=1}^{6}w_j^{n+1}\underbrace{\left(\int_\Omega\left(\sum_{j=1}^{6}{\lambda_2}_j^{n+1}\varphi_j^q\right)\frac{\partial\varphi_j^q}{\partial r}\frac{\partial\varphi_i^q}{\partial r}\,d\Omega\right)}_{\mathrm{LL}_{ij}}$$

$$+\Delta t\sum_{j=1}^{6}w_j^{n+1}\underbrace{\left(\int_\Omega\left(\sum_{j=1}^{6}{\lambda_2}_j^{n+1}\varphi_j^q\right)\frac{\partial\varphi_j^q}{\partial z}\frac{\partial\varphi_i^q}{\partial z}\,d\Omega\right)}_{\mathrm{LM}_{ij}}$$

$$-\Delta t\sum_{j=1}^{6}w_j^{n+1}\underbrace{\left(\int_\Omega\left(\sum_{j=1}^{6}{\lambda_2}_j^{n+1}\frac{\partial\varphi_j^q}{\partial z}\right)\frac{\partial\varphi_j^q}{\partial z}\varphi_i^q\,d\Omega\right)}_{\mathrm{DWZZ}_{ij}}\qquad(3.38)$$

$$-\Delta t\sum_{j=1}^{6}u_j^{n+1}\underbrace{\left(\int_\Omega\left(\sum_{j=1}^{6}{\lambda_2}_j^{n+1}\frac{\partial\varphi_j^q}{\partial r}\right)\frac{\partial\varphi_j^q}{\partial z}\varphi_i^q\,d\Omega\right)}_{\mathrm{DURZ}_{ij}}$$

$$-\frac{\Delta t}{CnCa}\sum_{j=1}^{6}\eta_j^{n+1}\underbrace{\left(\int_\Omega\left(\sum_{j=1}^{6}\phi_j^{n+1}\frac{\partial\varphi_j^q}{\partial z}\right)\varphi_j^q\varphi_i^q\,d\Omega\right)}_{\mathrm{KNPHIZ}_{ij}}$$

$$-\frac{Re(1-\rho)}{2}\sum_{j=1}^{6}\phi_j^{n+1}\underbrace{\left(\int_\Omega\left(\sum_{j=1}^{6}\mathrm{w}_j^n\varphi_j^q\right)\varphi_j^q\varphi_i^q\,d\Omega\right)}_{\mathrm{UW}_{ij}}$$

$$=\frac{Re(1+\rho)}{2}\sum_{j=1}^{6}\mathrm{w}_j^n\underbrace{\left(\int_\Omega\varphi_j^q\varphi_i^q\,d\Omega\right)}_{\mathrm{U}_{ij}}\Bigg]$$

$$\sum_{i=1}^{3}\bar{p}_i\Bigg[Re\sum_{j=1}^{6}u_j^{n+1}\underbrace{\left(\int_\Omega\frac{\partial\varphi_j^q}{\partial r}\varphi_i^l\,d\Omega\right)}_{\mathrm{PR1}_{ij}}+\sum_{j=1}^{6}u_j^{n+1}\underbrace{\left(\int_\Omega\frac{\varphi_j^q\varphi_i^l}{r}d\Omega\right)}_{\mathrm{OR}_{ij}}$$
$$+\sum_{j=1}^{6}w_j^{n+1}\underbrace{\left(\int_\Omega\frac{\partial\varphi_j^q}{\partial z}\varphi_i^l d\Omega\right)}_{\mathrm{PZ1}_{ij}}=0\Bigg] \tag{3.39}$$

$$\sum_{j=1}^{6}\bar{\phi}_i\Bigg[Re\sum_{j=1}^{6}\phi_j^{n+1}\underbrace{\left(\int_\Omega\varphi_j^q\varphi_i^q\,d\Omega\right)}_{\mathrm{U}_{ij}}$$

$$+\Delta t\sum_{j=1}^{6}u_j^{n+1}\underbrace{\left(\int_\Omega\left(\sum_{j=1}^{6}\phi_j^{n+1}\frac{\partial\varphi_j^q}{\partial r}\right)\varphi_j^q\varphi_i^q\,d\Omega\right)}_{\mathrm{KNPHIR}_{ij}}$$

$$+\Delta t\sum_{j=1}^{6}w_j^{n+1}\underbrace{\left(\int_\Omega\left(\sum_{j=1}^{6}\phi_j^{n+1}\frac{\partial\varphi_j^q}{\partial z}\right)\varphi_j^q\varphi_i^q\,d\Omega\right)}_{\mathrm{KNPHIZ}_{ij}} \tag{3.40}$$

$$+\frac{\Delta t}{Pe}\sum_{j=1}^{6}\eta_j^{n+1}\underbrace{\left(\int_\Omega\frac{\partial\varphi_j^q}{\partial r}\frac{\partial\varphi_i^q}{\partial r}d\Omega\right)}_{\mathrm{L}_{ij}}$$

$$+\frac{\Delta t}{Pe}\sum_{j=1}^{6}\eta_j^{n+1}\underbrace{\left(\int_\Omega \frac{\partial\varphi_j^q}{\partial z}\frac{\partial\varphi_i^q}{\partial z}\,d\Omega\right)}_{\mathrm{M}_{ij}}=\sum_{j=1}^{6}\phi_j^n\underbrace{\left(\int_\Omega \varphi_j^q\varphi_i^q\,d\Omega\right)}_{\mathrm{U}_{ij}}\Bigg]$$

$$\sum_{j=1}^{6}\bar{\eta}_i\Bigg[\sum_{j=1}^{6}\eta_j^{n+1}\underbrace{\left(\int_\Omega \varphi_j^q\varphi_i^q\,d\Omega\right)}_{\mathrm{U}_{ij}}+\sum_{j=1}^{6}\phi_j^{n+1}\underbrace{\left(\int_\Omega \varphi_j^q\varphi_i^q\,d\Omega\right)}_{\mathrm{U}_{ij}}$$

$$-\sum_{j=1}^{6}\phi_j^{n+1}\underbrace{\left(\int_\Omega\left(\sum_{j=1}^{6}\phi_j^{n+2}\varphi_i^q\right)^2\varphi_j^q\varphi_i^q\,d\Omega\right)}_{\mathrm{FF2}_{ij}}$$

$$-Cn^2\sum_{j=1}^{6}\phi_j^{n+1}\underbrace{\left(\int_\Omega \frac{\partial\varphi_j^q}{\partial r}\frac{\partial\varphi_i^q}{\partial r}\,d\Omega\right)}_{\mathrm{L}_{ij}} \tag{3.41}$$

$$-Cn^2\sum_{j=1}^{6}\phi_j^{n+1}\underbrace{\left(\int_\Omega \frac{\partial\varphi_j^q}{\partial z}\frac{\partial\varphi_i^q}{\partial z}\,d\Omega\right)}_{\mathrm{M}_{ij}}$$

$$=-Cn^2\underbrace{\left(\int_{\partial\Omega_b}(\boldsymbol{n}\nabla\phi)\varphi_i^q\,d\partial\Omega_b\right)}_{\mathrm{W}_i}\Bigg]$$

In more compact form, the components of the system to be solved are

$$Re\sum u_j^{n+1}\,\mathrm{LU}_{ij}+\Delta tRe\sum u_j^{n+1}\,\mathrm{LKNUR}_{ij}$$

$$+\Delta tRe\sum w_j^{n+1}\,\mathrm{LKNUZ}_{ij}+\Delta tRe\sum p_j^{n+1}\,\mathrm{PR}_{ij}$$

$$+\Delta t\sum u_j^{n+1}\,\mathrm{LL}_{ij}+\Delta t\sum u_j^{n+1}\,\mathrm{LM}_{ij}+\Delta t\sum u_j^{n+1}\,\mathrm{LR2}_{ij} \tag{3.42}$$

$$-\Delta t \sum u_j^{n+1}\,\mathrm{DURR}_{ij} - \Delta t \sum w_j^{n+1}\,\mathrm{DWZR}_{ij}$$
$$-\frac{\Delta t}{CnCa}\sum \eta_j^{n+1}\,\mathrm{KNPHIR}_{ij} - \frac{Re(1-\rho)}{2}\sum \phi_j^{n+1}\,\mathrm{UU}_{ij}$$
$$= \frac{Re(1+\rho)}{2}\sum \mathrm{u}_j^n\,\mathrm{U}_{ij}$$

$$Re\sum w_j^{n+1}\,\mathrm{LU}_{ij} + \Delta t Re\sum u_j^{n+1}\,\mathrm{LKNWR}_{ij}$$
$$+\Delta t Re\sum w_j^{n+1}\,\mathrm{LKNWZ}_{ij} + \Delta t Re\sum p_j^{n+1}\,\mathrm{PZ}_{ij}$$
$$+\Delta t\sum w_j^{n+1}\,\mathrm{LL}_{ij} + \Delta t\sum u_j^{n+1}\,\mathrm{LM}_{ij} + \Delta t\sum w_j^{n+1}\,\mathrm{LM}_{ij}$$
$$-\Delta t\sum w_j^{n+1}\,\mathrm{DWZZ}_{ij} - \Delta t\sum u_j^{n+1}\,\mathrm{DUZR}_{ij} \qquad (3.43)$$
$$-\frac{\Delta t}{CnCa}\sum \eta_j^{n+1}\,\mathrm{KNPHIZ}_{ij} - \frac{Re(1-\rho)}{2}\sum \phi_j^{n+1}\,\mathrm{UW}_{ij}$$
$$= \frac{Re(1+\rho)}{2}\sum \mathrm{w}_j^n\,\mathrm{U}_{ij}$$

$$\sum u_j^{n+1}\,\mathrm{PR1}_{ij} + \sum u_j^{n+1}\,\mathrm{OR}_{ij}\sum w_j^{n+1}\,\mathrm{PZ1}_{ij} = 0 \qquad (3.44)$$

$$\sum \phi_j^{n+1}\,\mathrm{U}_{ij} + \Delta t\sum u_j^{n+1}\,\mathrm{KNPHIR}_{ij} + \Delta t\sum w_j^{n+1}\,\mathrm{KNPHIZ}_{ij}$$
$$+\frac{\Delta t}{Pe}\sum \eta_j^{n+1}\,\mathrm{L}_{ij} + \frac{\Delta t}{Pe}\sum \eta_j^{n+1}\,\mathrm{M}_{ij} = \sum \phi_j^n\,\mathrm{U}_{ij} \qquad (3.45)$$

$$\sum \eta_j^{n+1} \mathrm{U}_{ij} + \sum \phi_j^{n+1} \mathrm{U}_{ij} + \sum \phi_j^{n+1} \mathrm{FF2}_{ij}$$
$$-Cn^2 \sum \phi_j^{n+1} \mathrm{L}_{ij} - Cn^2 \sum \phi_j^{n+1} \mathrm{M}_{ij} = -Cn^2 \mathrm{W}_i \tag{3.46}$$

Then all the set of equations are added onto a big matrix, the so-called stiffness matrix, $\boldsymbol{K}$, and right-hand side vector $\boldsymbol{R}$, namely $\boldsymbol{K}(\boldsymbol{s})\boldsymbol{s} = \boldsymbol{R}$. Demonstration of $\boldsymbol{K}(\boldsymbol{s})$ is given in Appendix A. We continue onwards with the boundary conditions of the system.

3.2 Implementation of Boundary Conditions

In this problem, the boundary conditions are in fact constraint relations, so we use the Lagrange multipliers method and extend the system of equations by adding Lagrange multipliers L for the restrictions,

$$\begin{bmatrix} \boldsymbol{K} & \boldsymbol{B^T} \\ \boldsymbol{B} & \boldsymbol{0} \end{bmatrix} \begin{bmatrix} U \\ L \end{bmatrix} = \begin{bmatrix} \boldsymbol{R} \\ u_i^* \end{bmatrix} \tag{3.47}$$

where $\boldsymbol{B}$ is a vector with all values equal to zero except its i^{th} entry which is equal to unity. u_i^* is the imposed constraint at node i. The constraints are no-slip boundary conditions at the rigid substrates, namely the u and w are set to zero. We also enforce u to be zero at the axisymmetry axis, $r = 0$. This method provides us with no to removel of columns/rows of the resulting system which is complicated for multi-dimensional problems. Fig 3.2 shows a summary of all the boundary conditions. Zero derivative based conditions require no implementation as the resulting surface integrals at the corresponding boundary vanish.

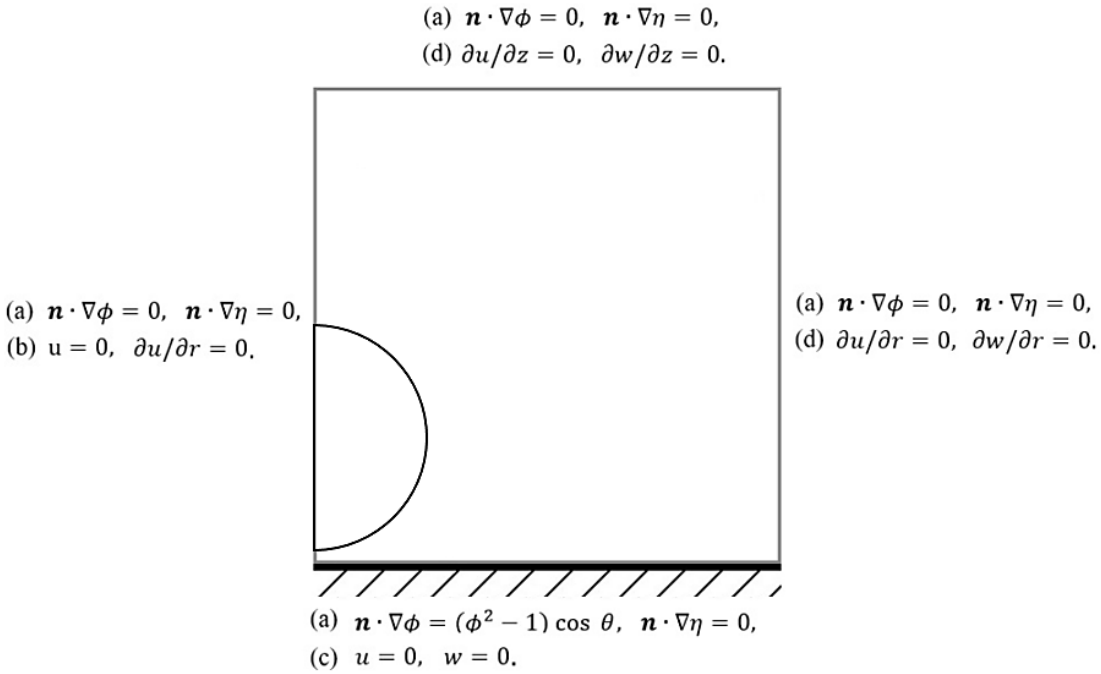

Figure.3.2: (a) Phase-field BC, (b) Symmetry BC,
(c) No-slip BC, (d) Stress–free BC.

We note that the treatment of wetting boundary condition is provided by the last integral in (3.41) by applying them into the specific nodes on the surface of droplet where the transition occurs from 1 to -1.

After the data is placed into the system, we plot the sparsity pattern as shown in Figure 3.3. It includes, in order of rows, $r-z$ momentum, continuity, Cahn-Hilliard and chemical potential equations contributions.

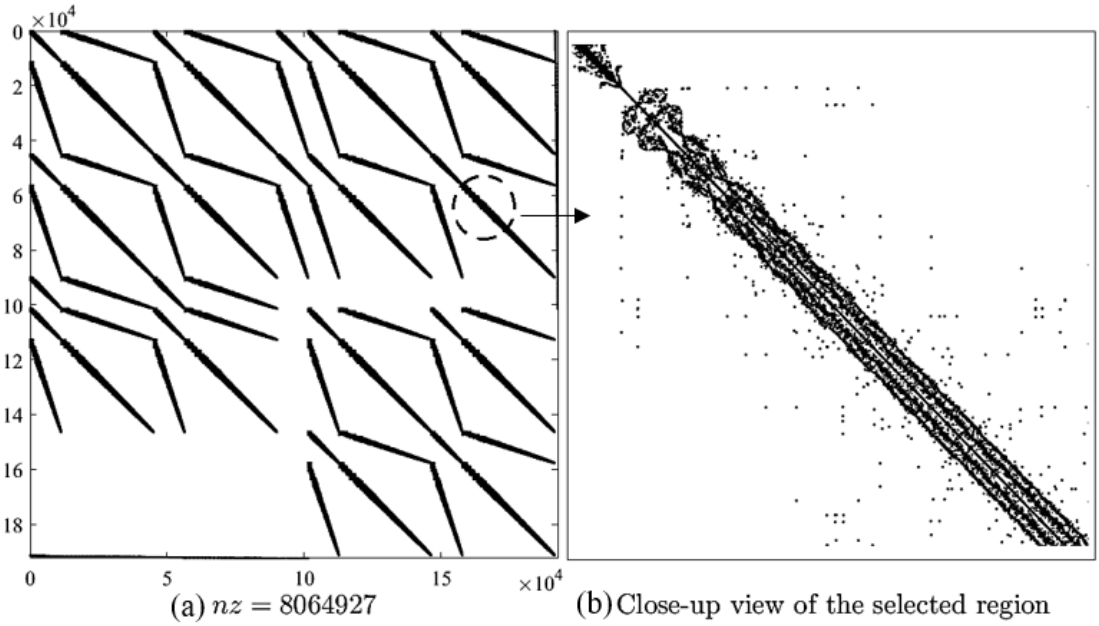

Figure 3.3: Sparsity pattern of resulting stiffness matrix, (a) full matrix with Dirichlet enforcement, the number of non-zero elements, *nz*, is about 8 million. (b) close-up view.

3.3 Treatment of Non-linear Terms

Because of the non-linear terms on the mass-acceleration in the momentum equations, the convective terms on the left-hand side of Cahn-Hilliard equation and the right-hand side of chemical potential equation, the stiffness matrix $\boldsymbol{K}$ has dependence on the unknown variables stored in $\boldsymbol{s}$. The system to be solved is

$$\boldsymbol{K}(\boldsymbol{s})\boldsymbol{s} = \boldsymbol{R}. \tag{3.48}$$

We define a residual vector as

$$\boldsymbol{r}(\boldsymbol{s}) = \boldsymbol{K}(\boldsymbol{s})\boldsymbol{s} - \boldsymbol{R} = 0 \tag{3.49}$$

which is a function of unknown vector $\boldsymbol{s}$. Finding the roots of $\boldsymbol{r}(\boldsymbol{s}) = 0$ provides us the solution at each time step which is also known as Newton's method and given by

$$\boldsymbol{s}^{m+1} = \boldsymbol{s}^{m} - \left[\frac{\partial \boldsymbol{r}}{\partial \boldsymbol{s}}\right]^{-1} [\boldsymbol{K}(\boldsymbol{s}^{m})\boldsymbol{s}^{m} - \boldsymbol{R}]. \tag{3.50}$$

This formulation requires evaluating the Tangent stiffness matrix, $\boldsymbol{T}$, and iteration until the difference between $\boldsymbol{s}^{m}$ and $\boldsymbol{s}^{m+1}$ is less than a tolerance. $\boldsymbol{T}$ is defined as

$$\boldsymbol{T}(\boldsymbol{u}) = \left[\frac{\partial \boldsymbol{r}}{\partial \boldsymbol{s}}\right]. \tag{3.51}$$

Chapter 4

Deformation of Drops Impacting onto Uniform Surfaces: Validation

We devote this chapter to validations and impact effects on chemically homogeneous surfaces. We give details on the deformation dynamics and scaling laws in Chapter 5.

4.1 Water and Ethanol Drops

We study two fundamental problems. The first one is the equilibrium shapes (static) of droplets on flat surfaces with uniform surface energy to check the accuracy of the wetting boundary condition if it satisfies the expected contact angles. We check partial wetting cases in the range of θ =30°to 150° and measured contact angles within a relative error of one degree. The other problem is the impact of drops onto surfaces with uniform wetting. For this purpose, we pick two different experimental studies, working with water and ethanol drops.

We, first, validate our solver for impact of water droplets over non-wetting but uniform surface energy substrates. To do this, we compare such physics with the experimental study of Rioboo [41]. A spherical water droplet diameter of $d = 3.3$ mm impacts with a velocity of $u = 1.18$ m/s onto a solid surface at a normal incidence. The equilibrium contact angle θ is uniform and 120°. The droplet has the density of 997 kg/m^3 and the viscosity of $1.\,10^{-3}$ Pa. s. For the ambient fluid, namely air, the density and the viscosity have values of 1.3 kg/m^3 and $1.\,7\ 10^{-5}$ Pa. s respectively. The drop-ambient fluid surface tension is $\gamma = 0{,}073$ N/m. With these parameters, we compute the non-dimensional numbers and summarize all in Table 4.1. The table also includes the Cahn

number, Cn, and Peclet number, Pe, which affects the resolution at the interface. We set Pe to $1/(3\,Cn)$ and the quadratic interpolation suggested in (2.19 - 2.20) is used for density and viscosity interpolations from one phase to another.

Table 4.1: Non-dimensional parameters for water.

Re	We	Cn	Ca	Pe	ρ	μ
3529.38	57.05	0.01	0.016	33.3	0.0013	0.017

We compare the experimental photographs and our results at the same times in Figure 4.1 with a good qualitative agreement.

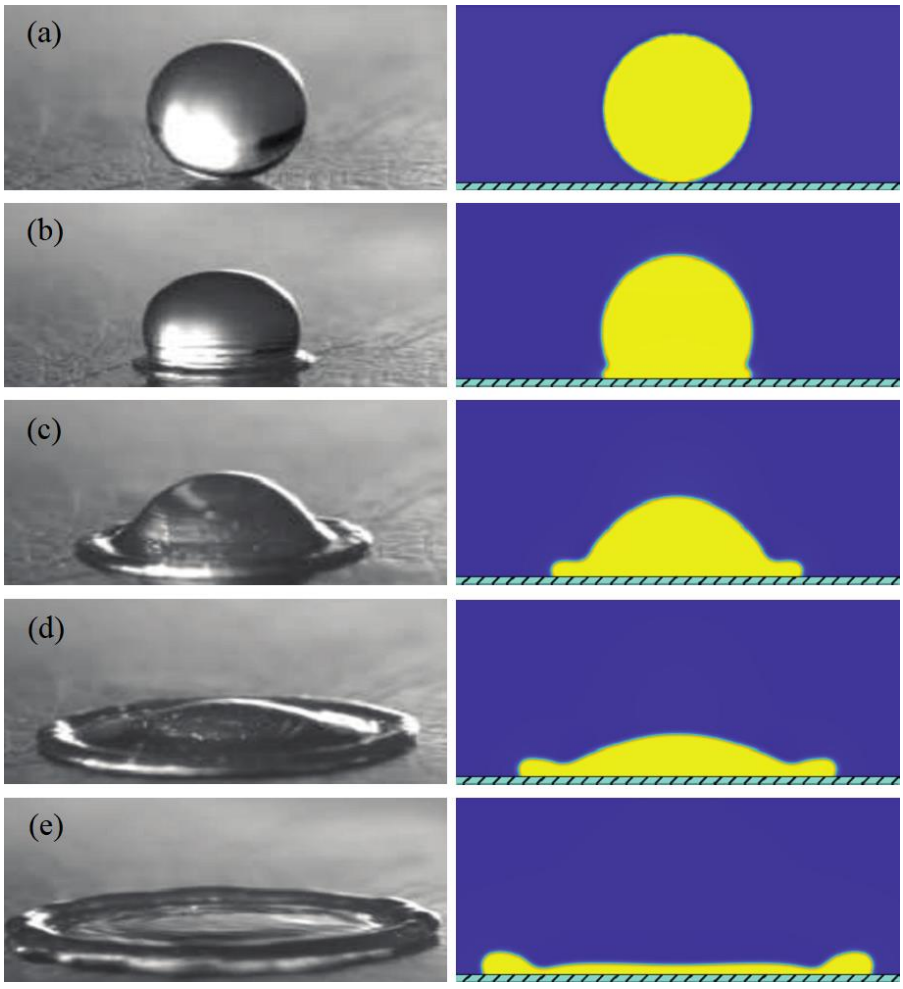

Figure 4.1: Time variation of water droplet profile at (a) $t^* = 0.0$ ms, (b) $t^* = 0.51$ ms, (c) $t^* = 1.31$ ms, (d) $t^* = 2.27$ ms, (e) $t^* = 4.71$ ms.

Our second validation is for an ethanol droplet surrounded with air from the study of Lee et al. [42]. Their parameters are, drop is of diameter $d = 2.0$ mm, which impacts with initial velocity of $u = 0.5$ m/s onto aluminum surface. The equilibrium contact angle θ chosen is uniform and set to its advancing dynamic value of $\theta = 59.8^o$. The droplet density is 789 kg/m^3 and the dynamic viscosity is $1.2\ 10^{-3}$ Pa. s. The air's density and the viscosity values are same for this case and was already given above. Liquid−gas surface tension value is $\gamma = 0{,}023$ N/m. The non-dimensional parameters are defined in Table 4.2.

Table 4.2: Non-dimensional parameters for ethanol.

Re	We	Cn	Ca	Pe	ρ	μ
657.5	17.15	0.01	0.016	33.3	0.0015	0.015

We compare our results with ethanol droplet in Figure 4.2. In both cases, the impact velocity is the velocity at the time t =0.

To be able to better explain the dynamics, we show the velocity vectors at several instances $t = 0.25$, $t = 0.75$, $t = 1.8$ in Figure 4.3 for the water drop. When the droplet meets the surface, it tries to attain the contact angle set with the surface while the inertia forces the interface to move sideways in the form of a jet as shown in panel (a) and (b). The fluid particles along the stagnation streamline, at $r = 0$, have the decelerate to stagnate at $z = 0$, while the remaining fluid particles follow a path similar to hyperbolas observed in classical stagnation point flow, which is clear from the velocity vectors of panel (b). The kinetic energy is converted partly to surface energy, and before the maximum extension, the start of receding is clearly seen in the magnified region of panel (c) near the contact line. We note the two recirculating regions. The furthest one from the incoming flow in the rim is the one near the contact line showing the motion is about the stop. The existence of a shear layer is also visible due to no-slip boundary condition. The effect of this layer on the fate of an impacting drop depends on the relative importance of Reynolds and Weber numbers that we discuss in the next chapter.

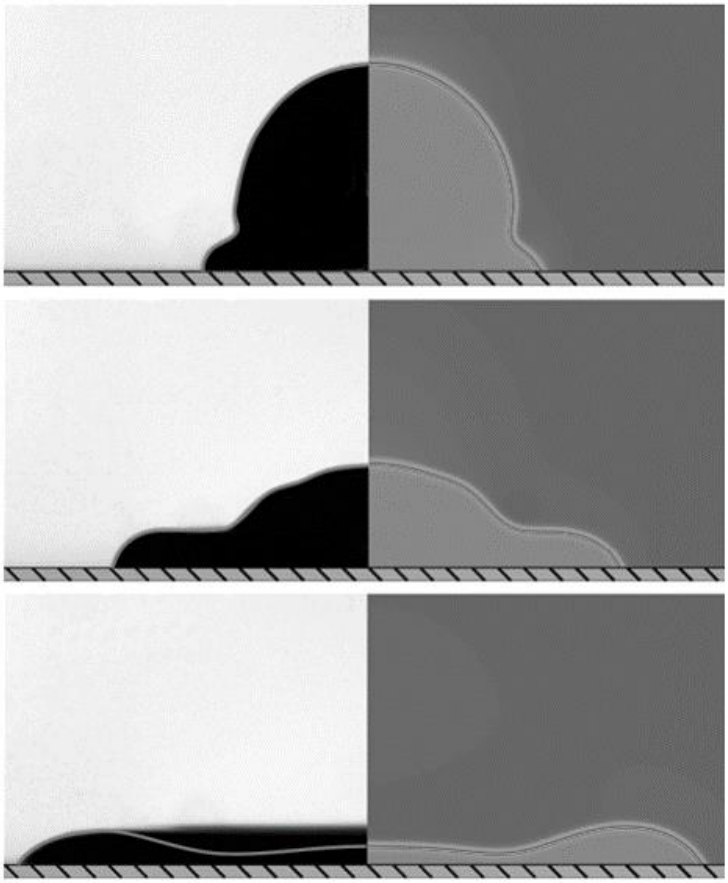

Figure 4.2: Deformation of ethanol droplet. Left panel is our computation, right panel is experiments of Lee et al. [42]. The times are (a) $t = 0.25$, (b) $t = 0.675$, (c) $t = 1.95$.

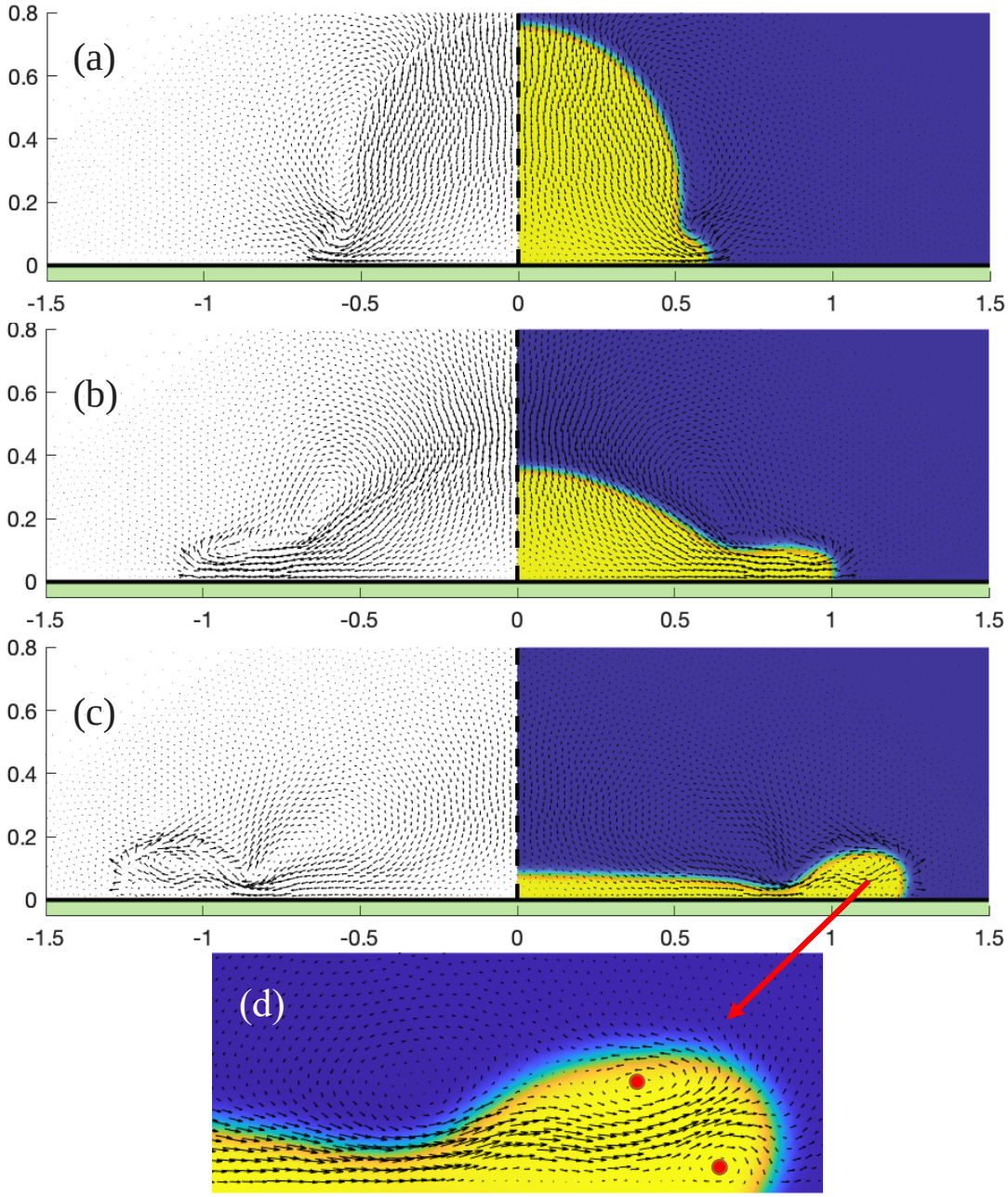

Figure 4.3: Deformation of water droplet. Left panel is our computation, right panel is experiments of Lee et al. [42]. The times are (a) $t = 0.25$, (b) $t = 0.75$, (c) $t = 1.8$, (d) magnified contact line region corresponding to (c).

4.2 Impact Regimes

The model problem is also capable of capturing different impact regimes. We show different regimes, defined in Table 1.3, of drop impact we observe with our solver in the following. We only show here two examples: complete rebound is shown in Figure

4.4 and splash is shown in Figure 4.5 with time frames with time intervals of 0.3. The parameters used for these cases are defined in Table 4.3 and 4.4.

Table 4.3: Non-dimensional parameters for complete rebound.

Re	We	Cn	Ca	Pe	ρ	μ
882.34	1.78	0.01	0.002	0.0054	0.0013	0.017

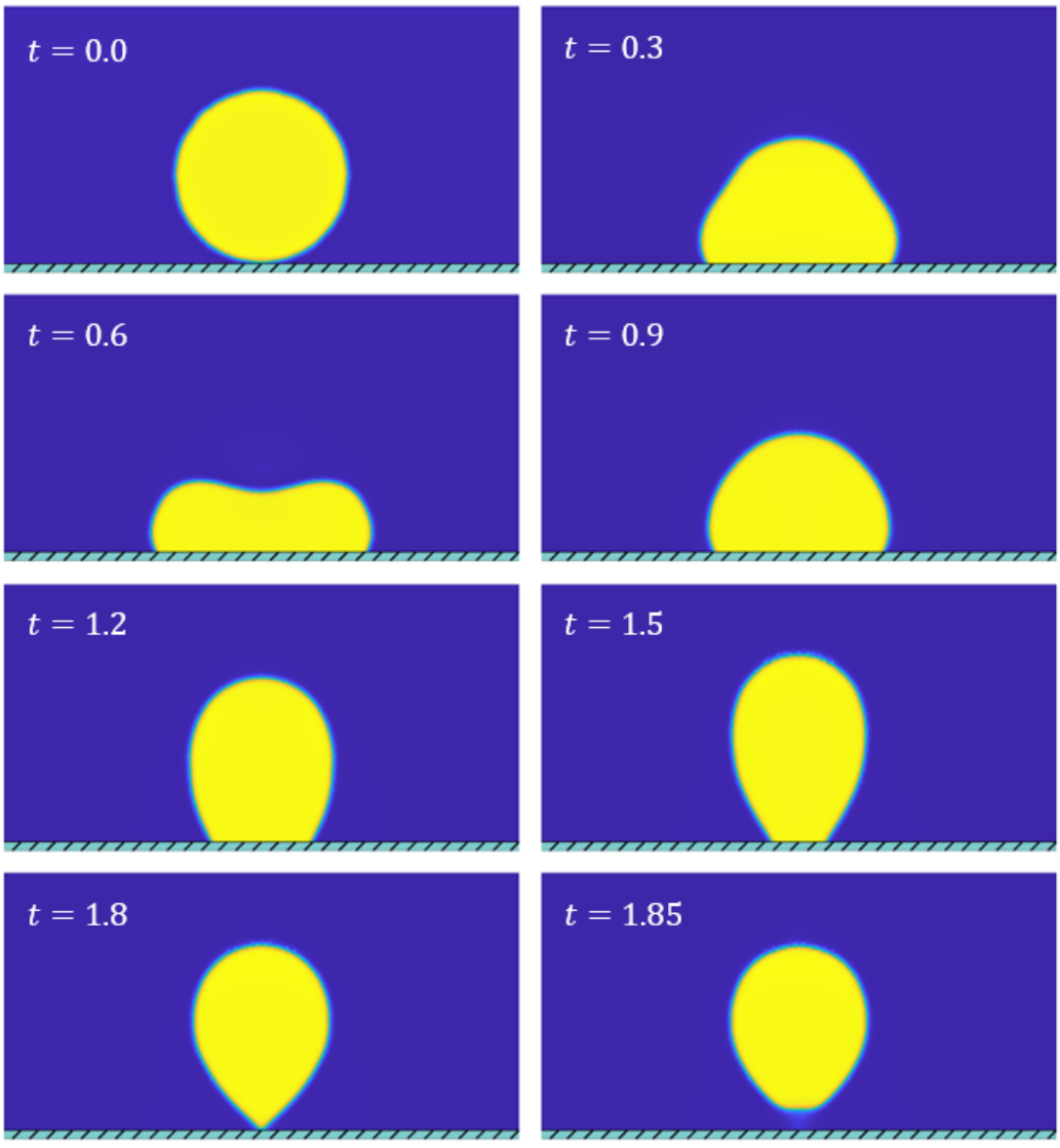

Figure 4.4: Time series for complete rebound.

Table 4.4: Non-dimensional parameters for splash.

Re	We	Cn	Ca	Pe	ρ	μ
7058.76	456.4	0.01	0.065	0.0054	0.0013	0.017

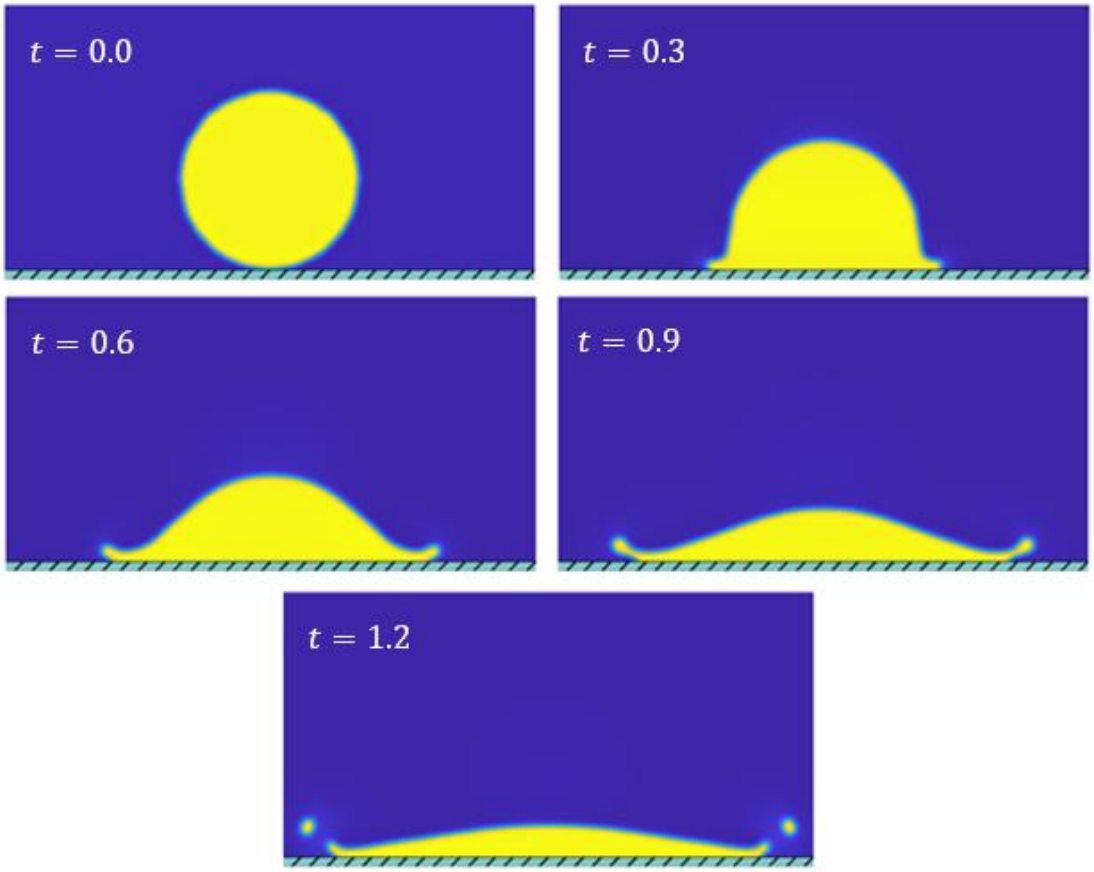

Figure 4.5: Time series for splash.

4.3 Mesh Structure

To end up with the comparisons given in Figure 4.1 and Figure 4.2, we first study the independence from mesh structure. The mesh resolutions for seven mesh structures are shown in Figure 4.6 and the number of elements and smallest mesh sizes are given in Table 4.5. The triangulation is structured in a way to increase the resolution in a region where drop deforms.

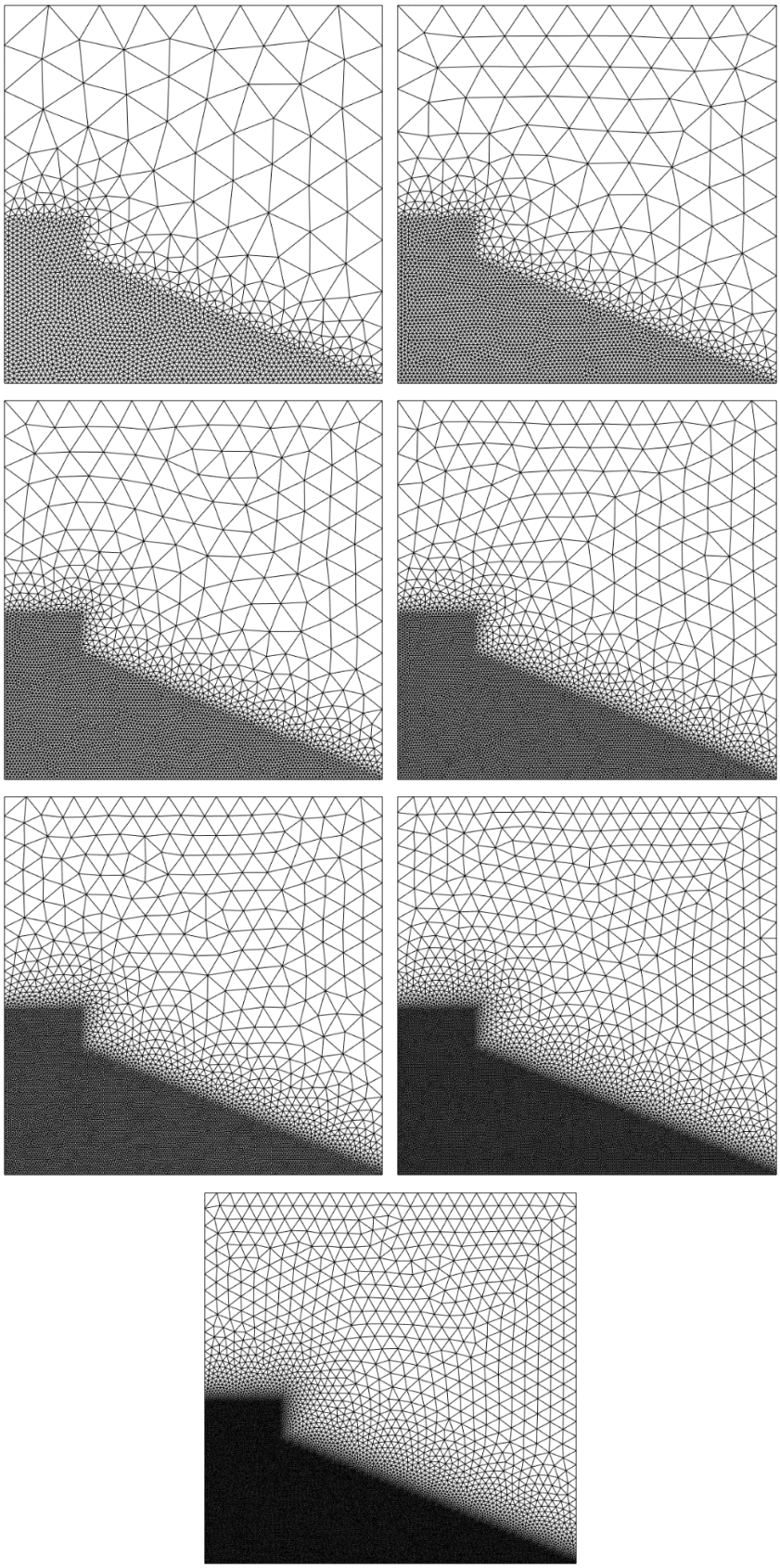

Figure 4.6: Mesh structure of the problem. Starting from coarse at the top left to fine at the bottom.

The representative meshes near the surface and around of the droplet are finer compared to the remaining of the domain due to critical regions. The domain is 2.5 by 2.5 in *r-z* directions. Because the length scale used in non-dimensionalization is the drops diameter, the fine region in the vertical covers a region of almost unit length; we reduce linearly the fine region to cover all solid and to make sure the drop is not deformed out of this region. The choice of this structure saves computational time.

In Table 4.5, we present the mesh information. T_h is the characteristic size of a triangulation in the fine region. Our coarsest mesh is named m_1. The finest mesh name is m_5. We systematically generate seven mesh structures in the order of decreasing element size.

Table 4.5: Mesh information used throughout the study.

Mesh name	Number of elements	T_h
m_1	3766	0.031885
m_2	5548	0.024881
m_3	8601	0.021251
m_{3-4}	11425	0.018207
m_4	15514	0.015166
m_{4-5}	22330	0.012803
m_5	34946	0.010604

We study the effect of mesh resolution by first observing the maximum extension diameter. We show the variation of d_{max} as function of t_h in Figure 4.7; again for the water case. The convergence suggests that resolution below m_{3-4} is not sufficient.

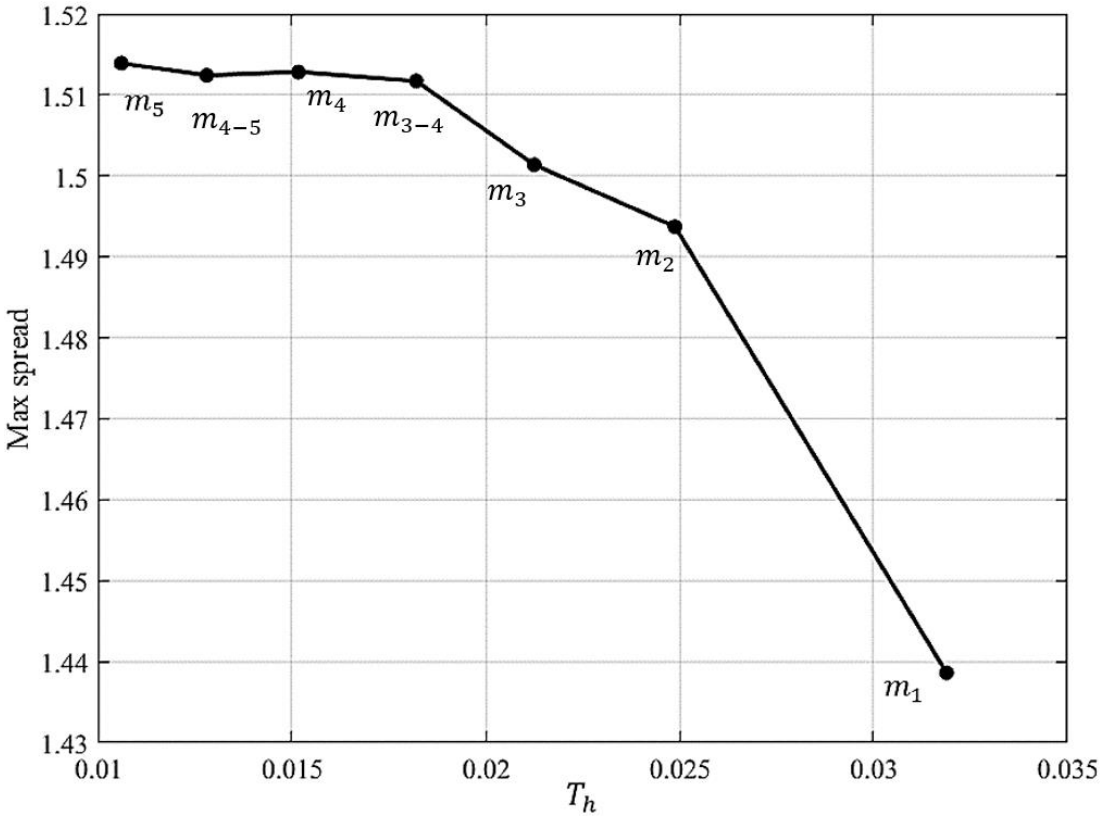

Figure 4.7: Independence from mesh for the maximum spreading.

We observe, however, that the effect of mesh on the mass conservation is more critical on the choice of mesh structure. Especially, the error in the computed volumes of liquid grows above 20% for the coarsest mesh at times $t = 3.0$ (t_4). The reason is due to under resolution of the interface and its diffusion with time. We show this variation in Figure 4.8.

We observe that from the average error of m_{3-4} on the $\boldsymbol{A}$ is about 2.1% since mass conservation within the liquid phase requires a higher resolution and $m_{3-4}$was also fine on the spreading data's so we decided use m_{4-5} for further runs. The mean error of rest of the group are error $m_1 = 9.7\%$, $m_2 = 6.47\%$, $m_3 = 3.71\%$, $m_{3-4} = 3.12\%$, $m_4 = 3.32\%$, $m_5 = 2.23\%$. Independent from the mesh, there is an increase of error with time. Mean errors of them are error $t_1 = 0.4721\%$, $t_2 = 2.6044\%$, $t_3 = 6.2185\%$, $t_4 = 6.2185\%$.

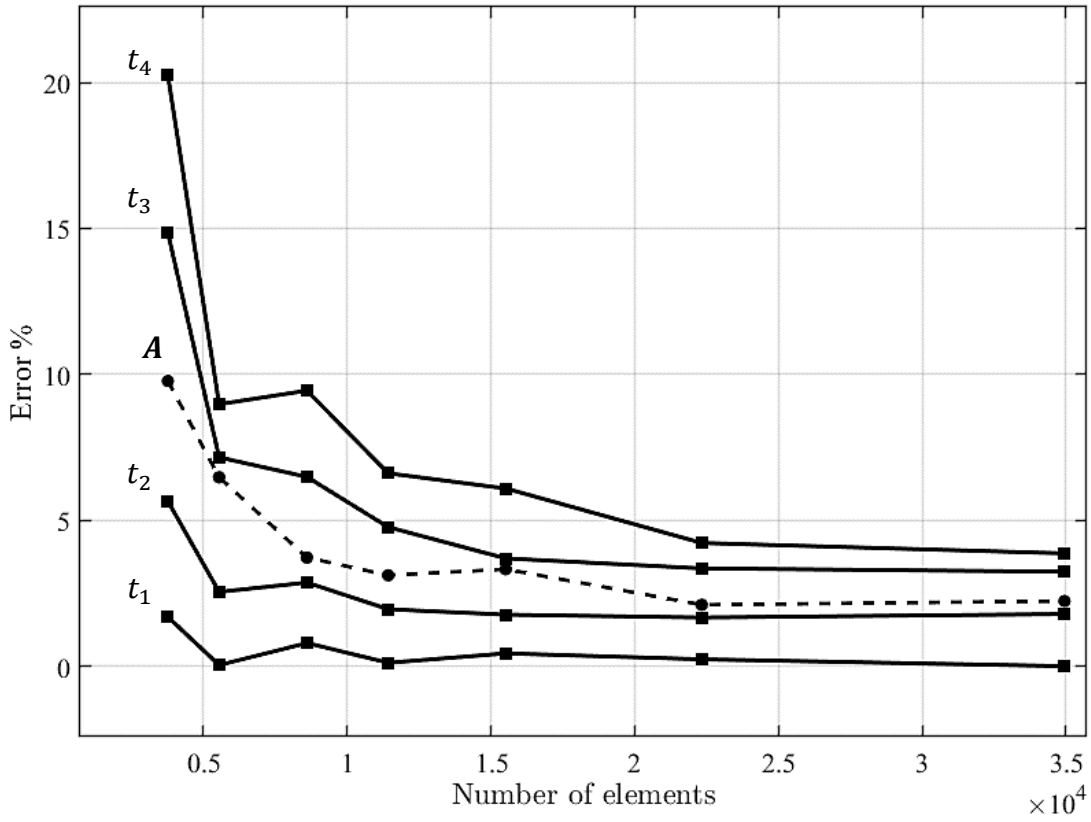

Figure 4.8: Error values at times $t_1 = 0.0$, $t_2 = 1.0$, $t_3 = 2.0$, $t_4 = 3.0$. $\boldsymbol{A}$ is the average of time values. In all cases squares represents meshes m_1 to m_5 toward right.

At different times, the volume computations are relatively misleading. The reason behind is the definition of the interface location to measure the volume, which also includes an error. We compute the volume of droplets by choosing the element nodes belonging to the liquid on the mesh. If elements six nodal points average satisfies $\phi > 1$, it is added to total volume (axisymmetric) of the drop. A representative triangulation is given below (Figure 4.9) for m_1 at time 0.59. We mark each element remaining in the liquid with a red star at the center of the elements. But even though this doesn't apply for all the time, the increase of element number decreases the percentage error.

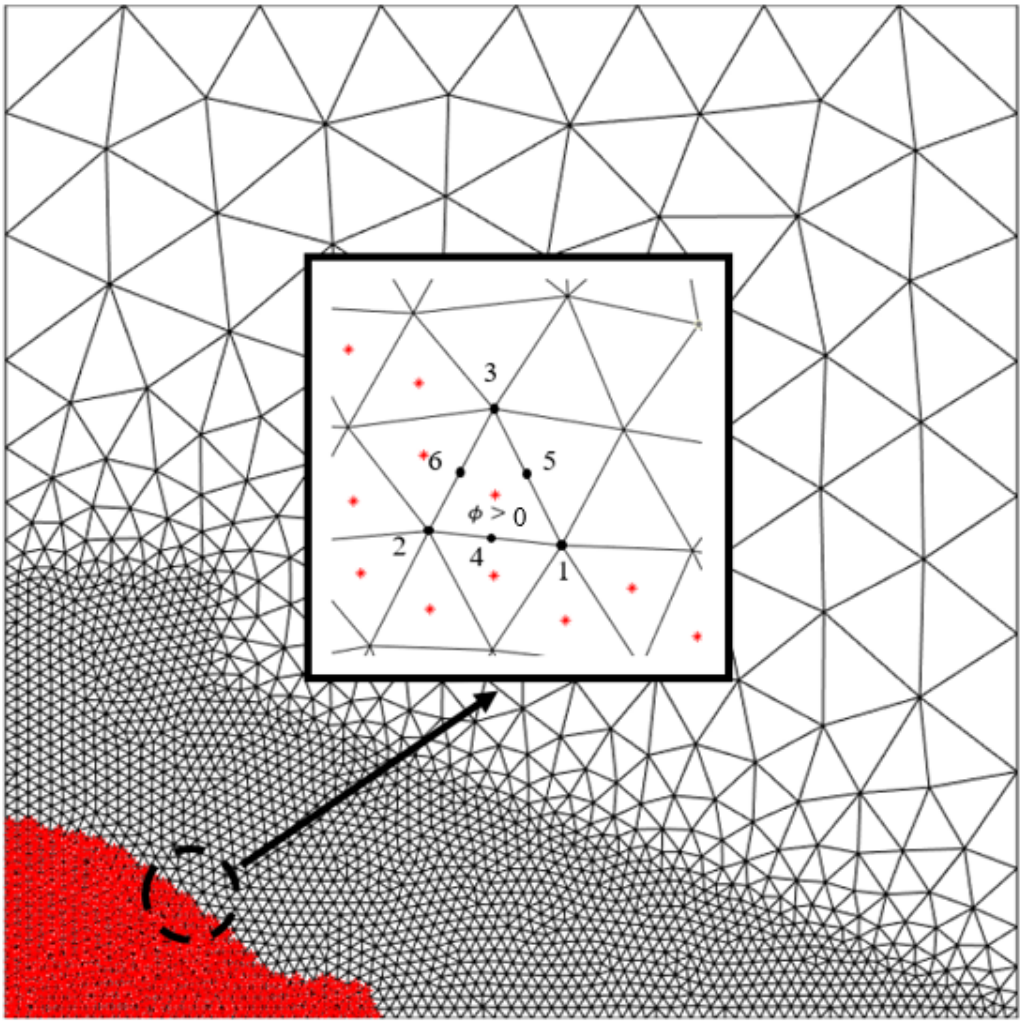

Figure 4.9: Volume traces of a solution.

4.4 Drop Impact Number

We finally compare if our computation captures the scaling law of an impacting drop as discussed in Clanet et. al [43]. There are two distinct regimes: namely capillary and viscous. The maximum extension,d_{max}, of a drop can be guessed on the grounds of energy balance that we discuss in the next chapter. The impact number $P = We/Re^{4/5}$ clearly separates the two regimes. When $P < 1$, the flow is in capillary regime and d_{max} follows a scaling law of $We^{1/4}$, otherwise the flow is in viscous regime and d_{max} follows a scaling law of $Re^{1/5}$. We show the comparison in Figure 4.10. d_{max} and d_o are the maximum extension of the drop and initial diameter of the drop. The symbols shown with black squares (■) are the Clanet's results while the ones shown

with red squares (■) are our results. The red triangles (▲) are different surface energy results that we discuss in the next chapter.

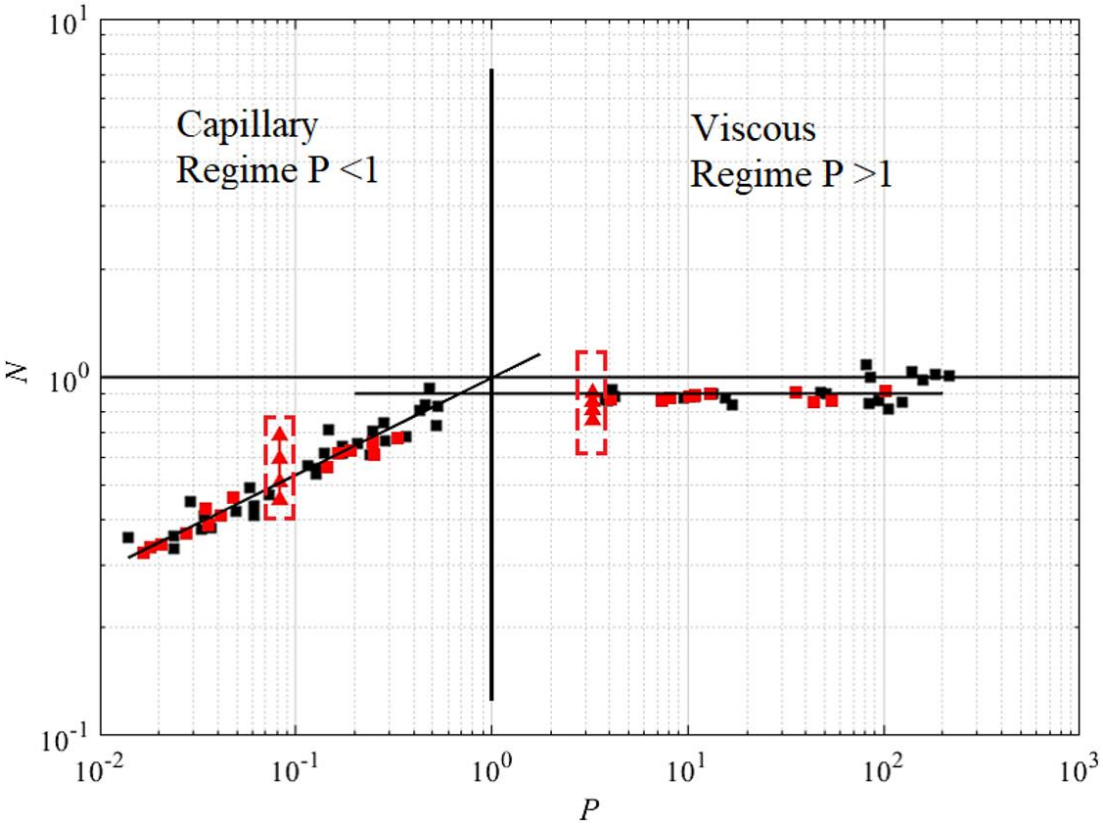

Figure 4.10: Scaling of maximum extension diameter of impacting drops, $N = d_{max}/(d_o Re^{1/5})$ vs. $P = We/Re^{4/5}$.

Chapter 5

Deformation of Drops Impacting onto Heterogeneous Surfaces

The deformation of an impacting drop onto surfaces may be altered if the surface structure is modified. This modification, for example, can be achieved by varying the chemical structure or the typography of the surface. In this chapter, we study the effect of structures on the deformation of an impacting drop onto a surface.

As explained earlier, the kinetic energy of the droplet before the impact is

$$E_U = \frac{1}{2}\rho U^2 \vartheta_d \tag{5.1}$$

where ρ is the density of droplet, U is the speed just before the impact and $\vartheta_d$is the volume of the droplet which is $\pi D^3/6$ in an axisymmetric nature. The surface energy of the same droplet, on the other hand is,

$$E_\gamma = \pi D^2 \gamma. \tag{5.2}$$

After the impact, part of the summation of the kinetic energy and surface energy is converted to surface energy due to varying interface shape, partly consumed by viscous deformation, may be converted onto other type of kinetic energy if there is still motion before or after the maximum extension. For an impacting drop onto uniform surface energy with flat interface, the scaling for this maximum extension can be guessed on the grounds of energy balance. For viscous regime (e.g. high viscosity

fluids may encounter such a situation), the nature of the deformation is determined by the viscous losses. One can integrate the viscous dissipation within the droplet volume over a course of time scaling with D/U, which is roughly

$$E_\eta = \phi_\eta \vartheta_d \frac{D}{U} \tag{5.3}$$

where ϕ_η is the viscous dissipation defined in index notation as

$$\phi_\eta = \eta \left(\frac{\partial u_i}{\partial x_j} + \frac{\partial u_j}{\partial x_i} \right) \frac{\partial u_i}{\partial x_j}. \tag{5.4}$$

In (5.4), $\partial u_i / \partial x_j$ is the velocity gradient, i, j are dummy indices meaning summation over the indices for three coordinate directions. (5.4) scales as $\eta(Uh)^2$ for a deformed droplet in a shape of pancake with corresponding height h and diameter d. For this shape, the volume can be estimated as

$$\vartheta = \frac{1}{4} \pi d^2 h. \tag{5.5}$$

The scaling for the viscous dissipation can then be written as

$$E_\eta \cong \frac{\pi \eta U D d^2}{4h}. \tag{5.6}$$

The volume conservation requires

$$\frac{1}{6} \pi D^3 = \frac{1}{4} \pi d^2 h \rightarrow D^3 = \frac{3}{2} d^2 h, \tag{5.7}$$

and if the kinetic energy of the initial state is consumed by the viscous dissipation, the diameter at the maximum extension would scale (when the viscous dissipation time scales as d/U) as

$$E_U(0) \sim E_\eta, \tag{5.8}$$

$$\rho U^2 D^3 \sim \frac{\eta U d_{max}^3}{h}, \tag{5.9}$$

$$\frac{\rho U D}{\eta} \sim \frac{d_{max}^5}{D^5}, \tag{5.10}$$

$$\frac{d_{max}}{D} \sim Re^{1/5}. \tag{5.11}$$

On the capillary regime, however; the acceleration $a \sim U^2/D$ of droplet is much larger than the gravitational acceleration for which the height of the droplet scales with capillary length $l \sim (\gamma/(\rho g))^{1/2}$. With this acceleration scale, the height scales then as

$$h \sim (\gamma/(\rho a))^{1/2} = (\gamma D/(\rho U^2))^{1/2}. \tag{5.12}$$

Using the volume conservation, we end up with

$$\frac{D^4}{d_{max}^4} \sim \frac{\gamma}{\rho U^2 D} \rightarrow \frac{d_{max}}{D} \sim We^{1/4}. \tag{5.13}$$

The energy conservation results with a scaling of $d_{max}/D \sim We^{1/2}$ which is a larger scaling than above.

The very first results of effect of surface energy variation is given in Figure 4.10. We vary the surface energy to satisfy uniform wetting angles of 150°, 120°, 90° and 60°. With the same non-dimensional properties; Re and We etc. but changing the chemical properties of the surface, we show the variation with red triangles in Figure. 4.10. We observe that the effect of increasing the surface energy (more wetting) is limited in the viscous regime ($P > 1$). This motivates us for further investigations for the alterations of the surface: generation of heterogeneities, either physical or chemical, in the capillary regime.

We search in this section if there is any change in the deformation if there is a structure at the surface. The droplet hits the pin-like structure(s) first then meet, if possible, the flat part of the surface. The idea is actually to answer the question whether the initial kinetic energy can be dissipated by the existence of such structures. To this end, we

systematically change the substrate typography by adding pin-like structures. We use reentrant structures with acute angles which we expect it increases the pinning at the corners. A representative axisymmetric drop on such structures is shown in Figure 5.1. Here, there are two structures one pin at the center and the other one is in the form of a ring. We increase the number of reentrant structures from 2 to 3 and 4 (which covers a length about unity which is approximately 0.3 less than the point of maximum extension over a flat surface).

The deformed interface shown in Figure. 5.1 is the water drop impacting used previously for validation purposes. The yellow is the droplet at $t = 1.6$, the green region is the structured surface. The liquid is not able to penetrate into the grooves, slides over the ambient fluid, pins at the leading edge of the last pin, and meets the flat surface.

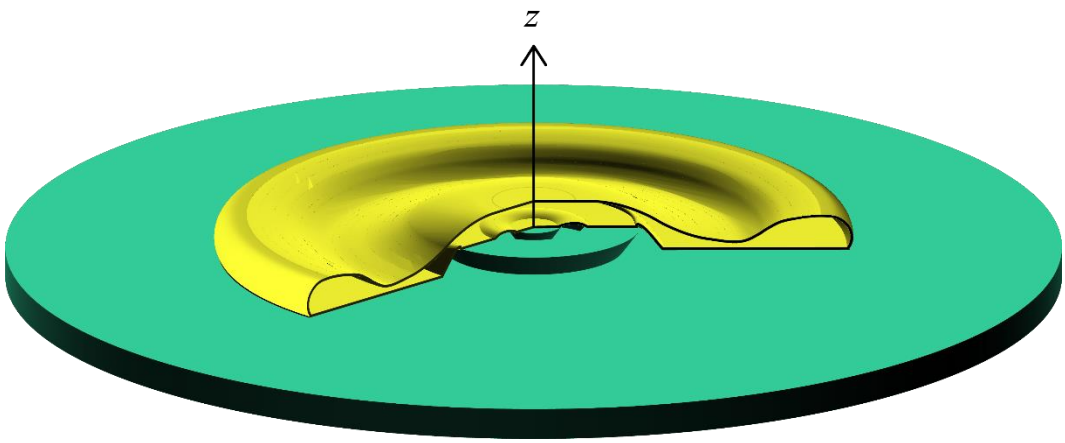

Figure 5.1: Droplet impacting onto structured surface.

For the following, we show only the symmetry plane. We, first, show the deformation of droplet for 2 and 3 structures at the same times in Figure. 5.2. The height of the structures is 0.1, with maximum width of 0.2 (top) and minimum width of 0.05 (bottom) and linear in between. The distance between each structure in radial direction is fixed and 0.3.

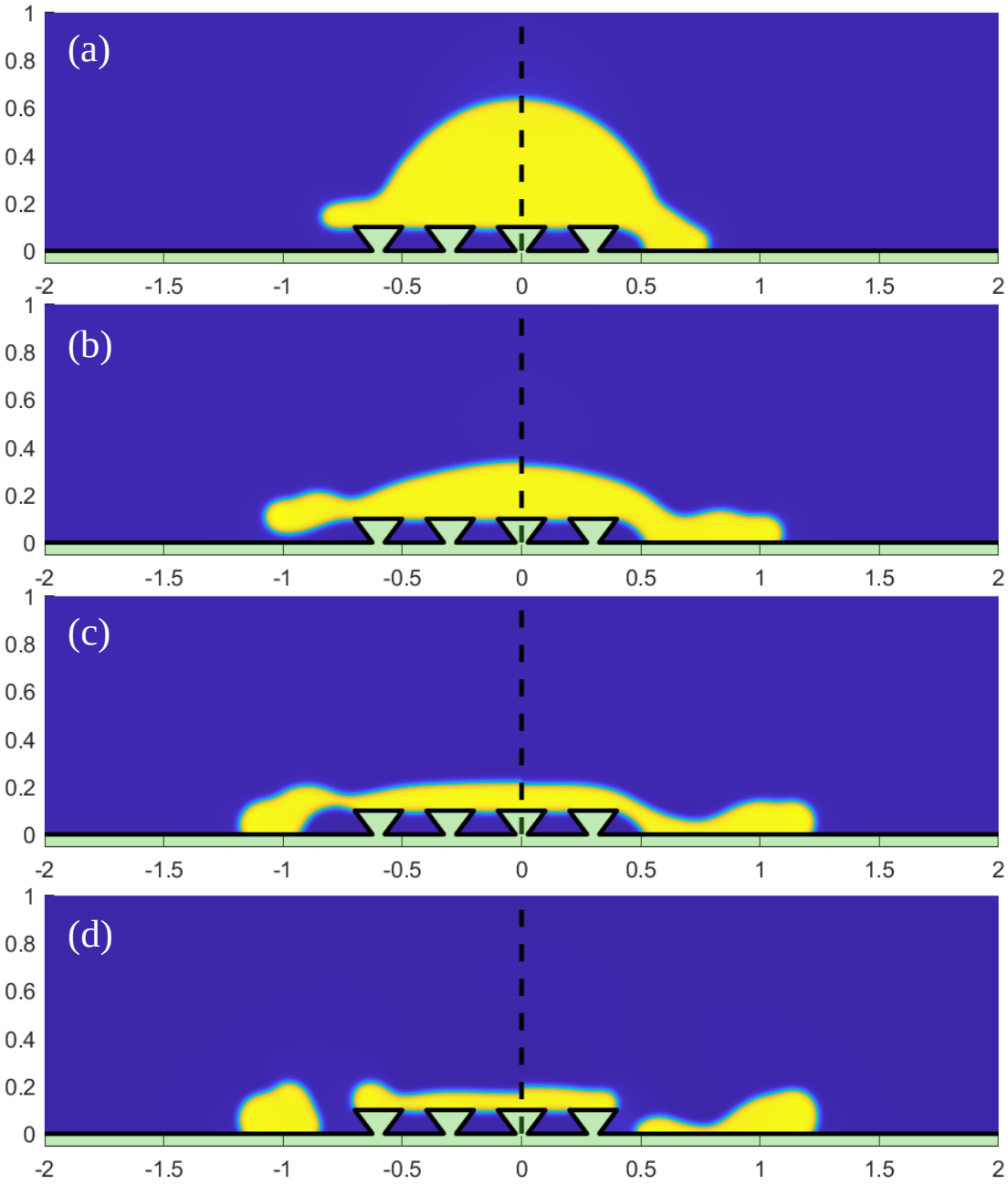

Figure 5.2: Comparison of 3-2 ring structures on the drop deformation, (a) $t = 0.5$, (b) $t = 1$, (c) $t = 1.5$, (d) $t = 2$.

The increase in the number of structures obviously slows down the motion. In Figure 5.2, the left and right panels show the effect of different number of structures on the drops deformation while (a) to (d) show the time evolution. The existence of corners provides drop break-up as seen in the right panel of Figure 5.2 (d). It occurs while the contact line advances over the flat part of the surface.

We validate this by increasing the number of pins and this time we compare 3 and 4 structures in Figure 5.3. Interestingly, over 4 structure case, the drop breaks-up over the structures, before touching the flat ground. The reasoning behind the slowing down of the motion is due to the increase of effective contact angles on such structures and pinning of the contact line at the corners of the reentrant rings.

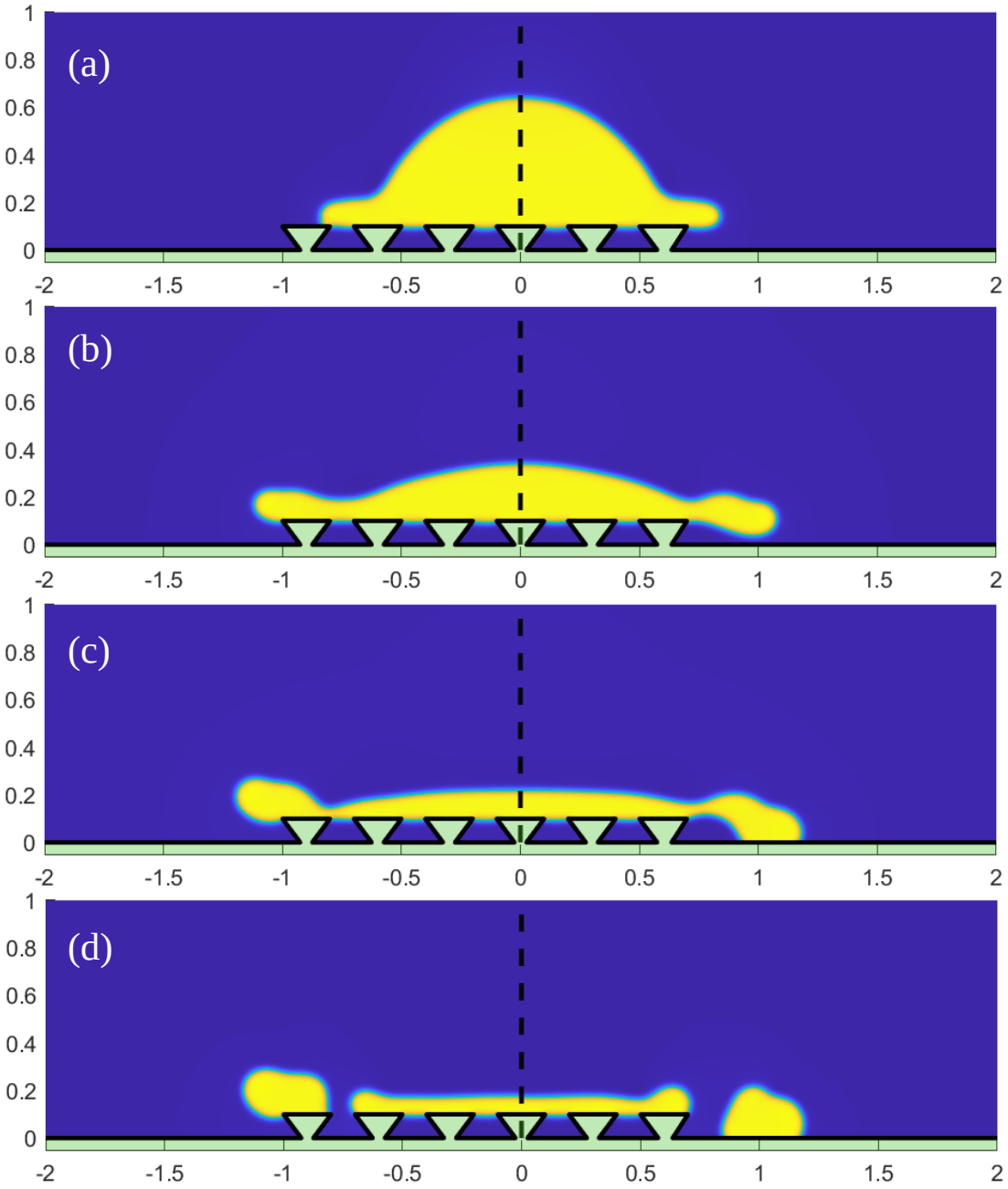

Figure 5.3: Comparison of 4-3 ring structures on the drop deformation, (a) $t = 0.5$, (b) $t = 1$, (c) $t = 1.5$, (d) $t = 2$.

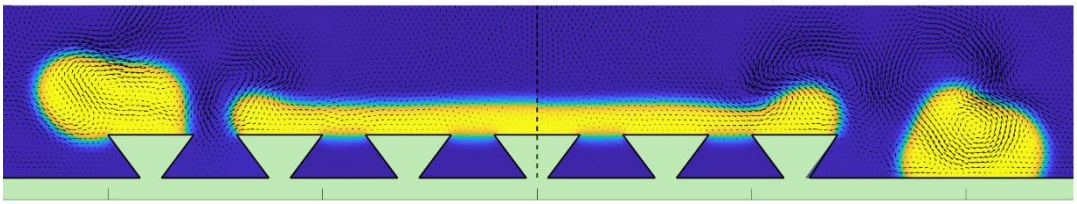

Figure 5.4: Velocity vectors corresponding to Figure. 5.3 (d).

In Figure. 5.4, we plot the velocity vectors just after the pinch-off, a ring from the end of drop over the 4-structure surface case (left panel). Over 3-structure surface (right panel), the interface breaks-up. The interface is not able to enter into the void in the reentrant structures; at the last ring, the interface is pinned at the corner which is also the case at the right panel after the pinch-off. After pinch-off, one part retracts as seen from the right arrows over the third structure while the other part seeks a possible equilibrium shape as is clear from the recirculation. A representative mesh structure behind the 4-structure solution is given in Figure 5.5.

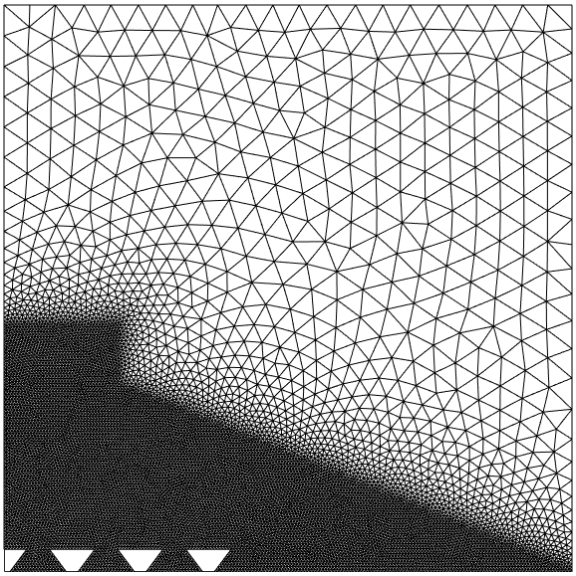

Figure 5.5: Mesh structure of roughness added surface.

Apart from the physical heterogeneity, we also change the wettability of the surface. The surface, now, is flat but contains varying wetting regions. We first study a case in which we observe splashing ring at the end of maximum extension. The parameters are $Re = 355$, $We = 919.7$, the density ratio and viscosity ratio are the same as water case. The choice of this specific Re and We is to observe splash. The substrate over which we observe the splash has a uniform wetting pattern with $\theta_e = 120^o$. The splash

starts around $r = 1.32$. In the neighborhood of this point, we change the wettability from $r = 0.8$ to $r = 1.3$ and set $\theta_e = 60^o$. The transition from $\theta_e = 120^o$ to $\theta_e = 60^o$ region is sharp and this region is actually in a form of ring due to axisymmetry. Smaller θ_e around this region would reduce the retarding force at the moving contact line and increases the spreading.

In Figure 5.6, we compare two cases at times $t = 0.0 - 0.9$ and in Figure 5.7, we show the later times at $t = 1.2 - 2.1$. The left panel is for the uniform surface energy case while the right panel is for varying wettability surface. We show that with this simple modification, we are able to prevent splash.

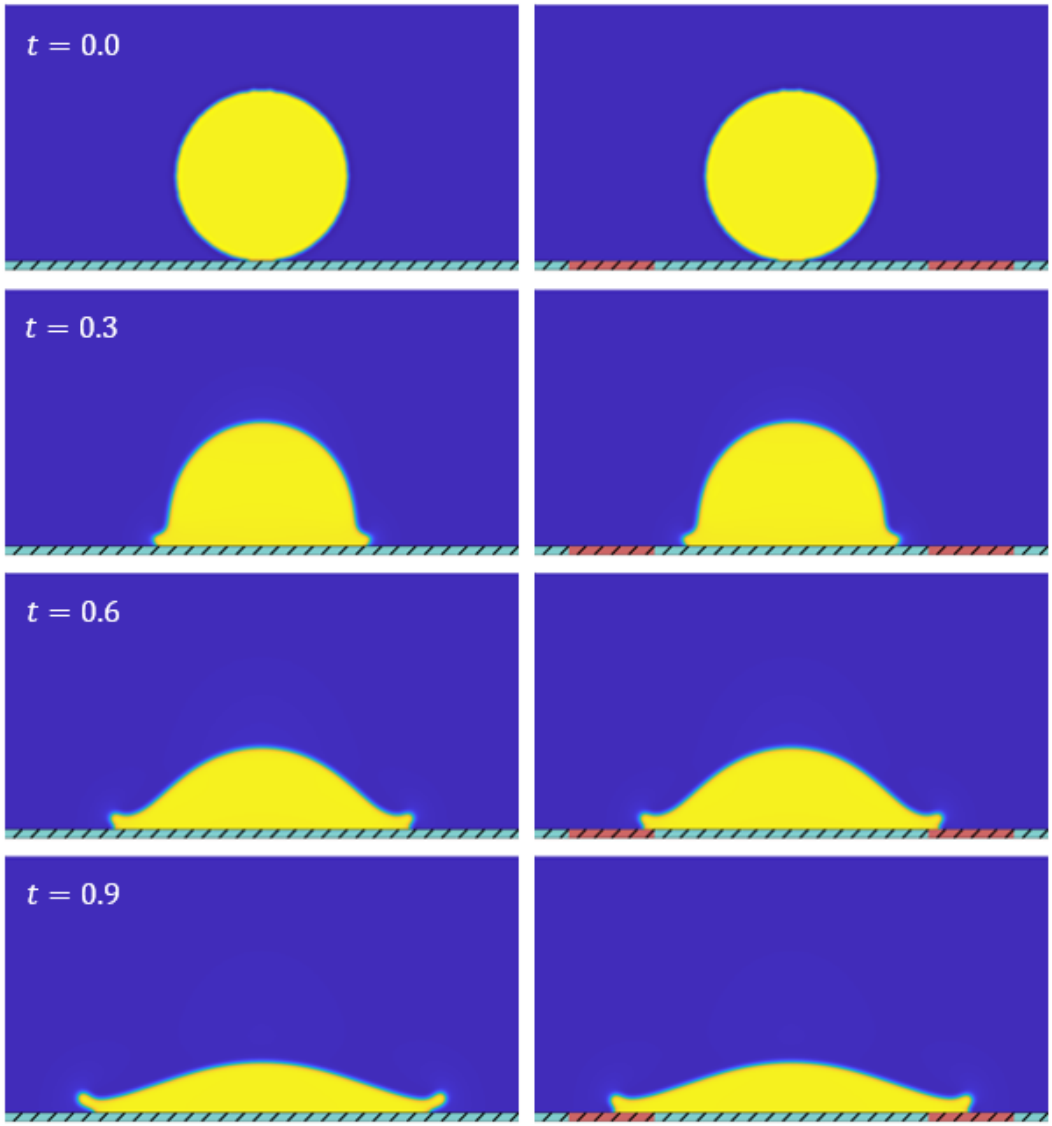

Figure 5.6: Comparison of wetting gradient on the drop deformation; left panel is for uniform surface; right panel is for non-uniform surface,
$t = 0.0$, $t = 0.3$, $t = 0.6$, $t = 0.9$.

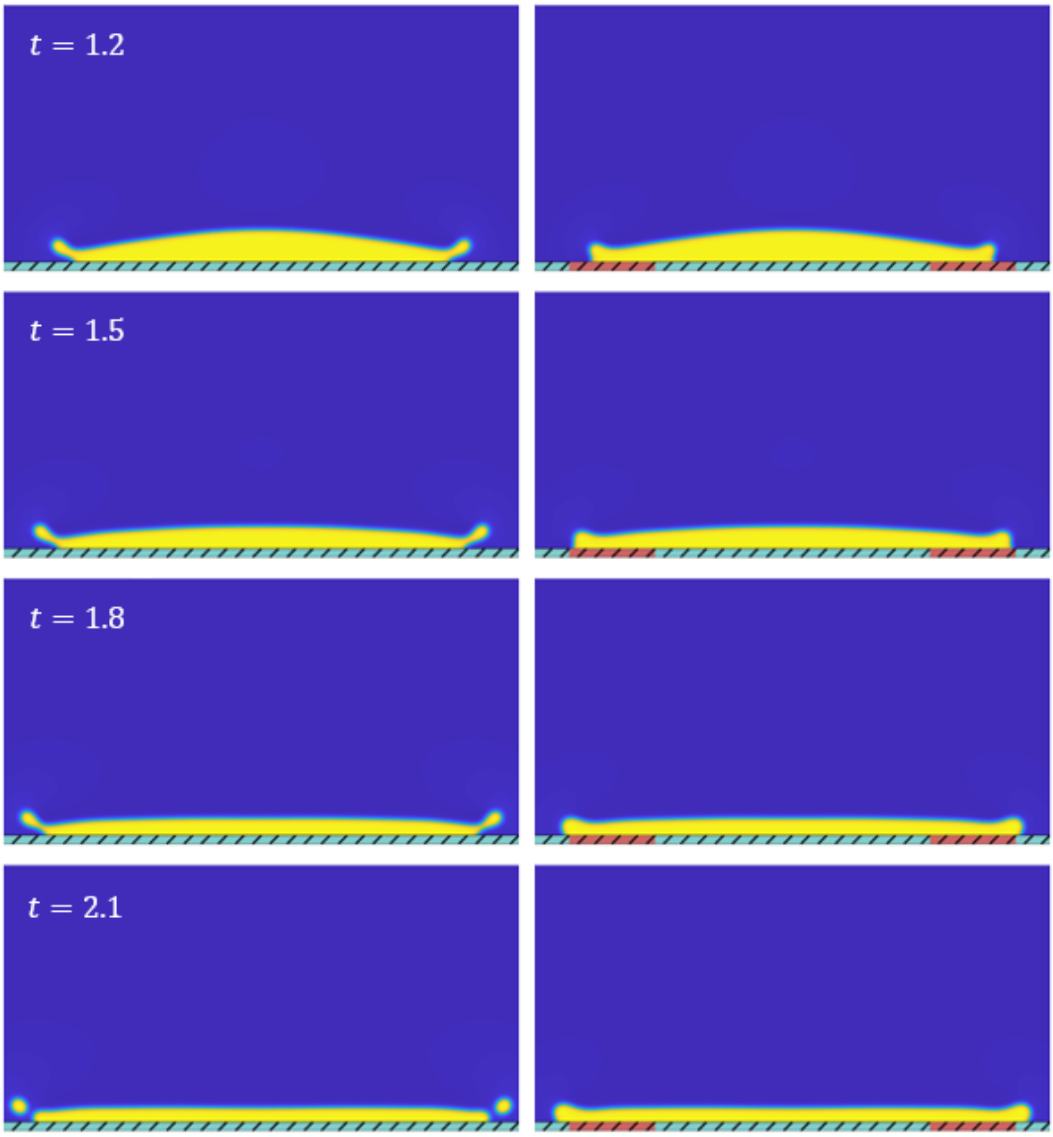

Figure 5.7: Later times of Fig. 5.6, $t = 1.2$, $t = 1.5$, $t = 1.8$, $t = 2.1$.

Chapter 6

Conclusion

We investigate the behavior of droplets impacting on surfaces with heterogeneities, specifically chemical applied surfaces and surface with roughness. With this purpose, we have developed an axisymmetric Navier-Stokes and Cahn-Hilliard multiphase flow model with FEM that can accurately predict droplet behavior on these surfaces, and have demonstrated the potential of using this model to design and control droplet-surface interactions. Through the combination of theoretical understandings and numerical simulations, we validate our model comparing with experiments and theoretical studies. The deformation obeys the power law relations of Re and We.

The observation of the wider spectrum of the effects of varying surface energy on the deformation within the capillary regime motivates us to seek for possible deformation with addition of new structures, rather than varying Re or We. We have discussed two main results: the effects of (i) physical structures (ii) chemical structures on the deformation of impacting drops. In the first scenario, we show how these structures retard the motion of the drops and enhance the pinch-off mechanism. In the second one, we have demonstrated that splash can be prevented by just playing with the wettability of the surfaces.

The simulations performed reveal various droplet-surface interactions and highlights the importance of considering the surface properties when designing and optimizing industrial processes that involve droplets. Though the geometry of the used structures is limited in the thesis, we believe the proposed model can be used as a tool to predict the behavior of droplets on various surfaces and can be used to optimize industrial processes. Overall, this thesis has made contribution to the field of multiphase flow, and has the potential to lead to the design of more efficient and effective surfaces.

References

[1] Worthington AM. On the forms assumed by drops of liquids falling vertically on a horizontal plate. Proceedings of the royal society of London 1877; 25(171-178): 261-272.

[2] Worthington AM. The splash of a drop. Society for Promoting Christian Knowledge; 1895.

[3] Taylor GI. The viscosity of a fluid containing small drops of another fluid. Proceedings of the Royal Society of London. Series A, Containing Papers of a Mathematical and Physical Character 1932; 138(834): 41-48.

[4] Grissom WM, Wierum FA. Liquid spray cooling of a heated surface. International Journal of Heat and Mass Transfer 1981; 24(2): 261-271.

[5] Kim J. Spray cooling heat transfer: The state of the art. International Journal of Heat and Fluid Flow 2007; 28(4): 753-767.

[6] Park J, Moon J. Control of colloidal particle deposit patterns within picoliter droplets ejected by ink-jet printing. Langmuir 2006; 22(8): 3506-3513.

[7] Bergeron V, Quéré D. Water droplets make an impact. Physics world 2001; 14(5): 27.

[8] Attinger D, Zhao Z, Poulikakos D. An experimental study of molten microdroplet surface deposition and solidification: transient behavior and wetting angle dynamics. J. Heat Transfer 2000; 122(3): 544-556.

[9] Maier C, Wiesche S, Hofer EP. Impact of microdrops on solid surfaces for DNA-synthesis. In Proceedings of the 2000 international conference on modeling and simulation of microsystems 2000: 586-589.

[10] De Gennes PG, Brochard-Wyart F, Quéré D. Capillarity and wetting phenomena: drops, bubbles, pearls, waves 2004; (Vol. 315). New York: Springer: 15.

[11] Young T. An essay on the cohesion of fluids (Phil. Trans. 1805. P.65). In Abstracts of the Papers Printed in the Philosophical Transactions of the Royal Society of London (No. 1, pp. 171-172). London: The Royal Society 1832.

[12] Poisson SD. Nouvelle théorie de l'action capillaire 1831.

[13] Rowlinson JS, Widom B. Molecular theory of capillarity. Courier Corporation 2013.

[14] Law KY, Zhao H. Surface wetting: characterization, contact angle, and fundamentals. Basel, Switzerland: Springer International Publishing 2016.

[15] Berry MV. The molecular mechanism of surface tension. Physics Education 1971, 6(2): 79.

[16] Marchand A, Weijs JH, Snoeijer JH, Andreotti B. Why is surface tension a force parallel to the interface?. American Journal of Physics 2011; 79(10): 999-1008.

[17] Coffinier Y, Piret G, Das MR, Boukherroub R. Effect of surface roughness and chemical composition on the wetting properties of silicon-based substrates. Comptes Rendus Chimie 2013; 16(1): 65-72.

[18] Van Oss CJ. Hydrophobicity and hydrophilicity of biosurfaces. Current opinion in colloid & interface science 1997; 2(5): 503-512.

[19] Law KY. Definitions for hydrophilicity, hydrophobicity, and superhydrophobicity: getting the basics right. The Journal of Physical Chemistry Letters 2014; 5(4): 686-688.

[20] Ellis AS, Smith FT, White AH. Droplet impact on to a rough surface. The Quarterly Journal of Mechanics & Applied Mathematics 2011; 64(2): 107-139.

[21] Giacomello A, Meloni S, Chinappi M, Casciola CM. Cassie–Baxter and Wenzel states on a nanostructured surface: phase diagram, metastabilities, and transition mechanism by atomistic free energy calculations. Langmuir 2012; , 28(29): 10764-10772.

[22] Rioboo R, Tropea C, Marengo M. Outcomes from a drop impact on solid surfaces. Atomization and sprays 2001; 11(2).

[23] Yarin AL. Drop impact dynamics: splashing, spreading, receding, bouncing… Annual review of fluid mechanics 2006; 38(1): 159-192.

[24] Tsai P, Pacheco,S, Pirat C, Lefferts L, Lohse D. Drop impact upon micro-and nanostructured superhydrophobic surfaces. Langmuir 2009; 25(20): 12293-12298.

[25] Bundy FP, Bassett WA, Weathers MS, Hemley RJ, Mao HU, Goncharov AF. The pressure-temperature phase and transformation diagram for carbon; updated through 1994 1996; Carbon, 34(2): 141-153.

[26] Su Y, Landis CM. Continuum thermodynamics of ferroelectric domain evolution: Theory, finite element implementation, and application to domain wall pinning. Journal of the Mechanics and Physics of Solids 2007; 55(2): 280-305.

[27] Yue P, Feng JJ, Liu C, Shen J. A diffuse-interface method for simulating two-phase flows of complex fluids. Journal of Fluid Mechanics 2004; 515: 293-317.

[28] Scardovelli R, Zaleski S. Direct numerical simulation of free-surface and interfacial flow. Annual review of fluid mechanics 1999; 31(1): 567-603.

[29] Hirt CW, Nichols BD. Volume of fluid (VOF) method for the dynamics of free boundaries. Journal of computational physics 1981; 39(1): 201-225.

[30] Badalassi VE, Ceniceros HD, Banerjee S. Computation of multiphase systems with phase field models. Journal of computational physics 2003; 190(2): 371-397.

[31] Osher S, Sethian JA. Fronts propagating with curvature-dependent speed: Algorithms based on Hamilton-Jacobi formulations. Journal of computational physics 1988; 79(1): 12-49.

[32] Gomez H, Hughes TJ, Nogueira X, Calo VM. Isogeometric analysis of the isothermal Navier–Stokes–Korteweg equations. Computer Methods in Applied Mechanics and Engineering 2010; 199(25-28): 1828-1840.

[33] Cahn JW, Hilliard JE. Free energy of a nonuniform system. I. Interfacial free energy. The Journal of chemical physics 1958; 28(2): 258-267.

[34] Cahn JW, Allen SM. A microscopic theory for domain wall motion and its experimental verification in Fe-Al alloy domain growth kinetics. Le Journal de Physique Colloques 1977; 38(C7): C7-51.

[35] Kim J. A continuous surface tension force formulation for diffuse-interface models. Journal of Computational Physics 2005; 204(2): 784-804.

[36] Liu C, Shen J. A phase field model for the mixture of two incompressible fluids and its approximation by a Fourier-spectral method. Physica D: Nonlinear Phenomena 2003; 179(3-4): 211-228.

[37] Jacqmin, D. Contact-line dynamics of a diffuse fluid interface. Journal of fluid mechanics 2000; 402: 57-88.

[38] Joseph DD, Renardy YY. Fundamentals of two-fluid dynamics: part II: lubricated transport, drops and miscible liquids (Vol. 4). Springer Science & Business Media 2013.

[39] Caffarelli LA, Muler NE. An L^{∞} bound for solutions of the Cahn-Hilliard equation. Archive for rational mechanics and analysis 1995; 133(2): 129-144.

[40] Badalassi VE, Banerjee S. Nano-structure computation with coupled momentum phase ordering kinetics models. Nuclear engineering and design 2005; 235(10-12): 1107-1115.

[41] Rioboo R. ‘Impact de gouttes sur surfaces solides et sèches’, thèse à l’université Paris 6, 2001.

[42] Lee JB, Derome D, Guyer R, Carmeliet J. Modeling the maximum spreading of liquid droplets impacting wetting and nonwetting surfaces. Langmuir 2016; 32(5): 1299-1308.

[43] Clanet C, Béguin C, Richard D, Quéré D. Maximal deformation of an impacting drop. Journal of Fluid Mechanics 2004; 517: 199-208.

Appendices

Appendix A

The stiffness matrix $\boldsymbol{K}$

$$\underbrace{\begin{bmatrix} Re\mathrm{LU}_{ij}+\Delta t(Re\mathrm{LKNUR}_{ij} \\ +\mathrm{LL}_{ij}+\mathrm{LM}_{ij}+\mathrm{LR2}_{ij}-\mathrm{DURR}_{ij}) & \Delta t\left(Re\mathrm{LKNUZ}_{ij}-\mathrm{DWRZ}_{ij}\right) & \Delta t\mathrm{PR}_{ij} & -\frac{Re(1-\rho)}{2}\mathrm{UU}_{ij} & -\frac{\Delta t}{CnCa}\mathrm{KNPHIR}_{ij} \\ \Delta t\left(Re\mathrm{LKNWR}_{ij}-\mathrm{DURZ}_{ij}\right) & Re\mathrm{LU}_{ij}+\Delta t(Re\mathrm{LKNWZ}_{ij} \\ & +\mathrm{LL}_{ij}+\mathrm{LM}_{ij}-\mathrm{DWZZ}_{ij}) & \Delta t\mathrm{PZ}_{ij} & -\frac{Re(1-\rho)}{2}\mathrm{UW}_{ij} & -\frac{\Delta t}{CnCa}\mathrm{KNPHIZ}_{ij} \\ \mathrm{PR1}_{ij}+\mathrm{OR}_{ij} & \mathrm{PZ1}_{ij} & 0 & 0 & 0 \\ \Delta t\ \mathrm{KNPHIR}_{ij} & \Delta t\ \mathrm{KNPHIZ}_{ij} & 0 & \mathrm{U}_{ij} & \frac{\Delta t}{Pe}(\mathrm{L}_{ij}+\mathrm{M}_{ij}) \\ 0 & 0 & 0 & \mathrm{U}_{ij}-\mathrm{FF2}_{ij} \\ & & & -Cn^2(\mathrm{L}_{ij}+\mathrm{M}_{ij}) & \mathrm{U}_{ij} \end{bmatrix}}_{\mathrm{K}_{ij}(\mathrm{s}_j)} \underbrace{\begin{bmatrix} u_j^{n+1} \\ w_j^{n+1} \\ p_j^{n+1} \\ \phi_j^{n+1} \\ \eta_j^{n+1} \end{bmatrix}}_{\mathrm{s}_j} = \underbrace{\begin{bmatrix} \frac{Re(1+\rho)}{2}\mathrm{u}_j^n\mathrm{U}_{ij} \\ \frac{Re(1+\rho)}{2}\mathrm{w}_j^n\mathrm{U}_{ij} \\ 0 \\ \phi_j^n\mathrm{U}_{ij} \\ -Cn^2\mathrm{W}_i \end{bmatrix}}_{\mathrm{R}_i} \tag{A.1}$$